Characterization and Modeling of Erbium-Doped Fiber Amplifiers and Impact of Fiber Dispersion on Semiconductor Laser Noise

By

MAHAN MOVASSAGHI

B.Sc. Amir-Kabir University of Technology, Tehran, Iran, 1992
M.A.Sc. University of British Columbia, Vancouver, Canada, 1996

A THESIS SUBMITTED IN PARTIAL FULFILMENT OF THE REQUIREMENTS FOR THE DEGREE OF

DOCTOR OF PHILOSOPHY

in

THE FACULTY OF GRADUATE STUDIES

Department of Electrical and Computer Engineering

We accept this thesis as conforming
to the required standard

THE UNIVERSITY OF BRITISH COLUMBIA

July 1999

In presenting this thesis in partial fulfilment of the requirements for an advanced degree at the University of British Columbia, I agree that the Library shall make it freely available for reference and study. I further agree that permission for extensive copying of this thesis for scholarly purposes may be granted by the head of my department or by his or her representatives. It is understood that copying or publication of this thesis for financial gain shall not be allowed without my written permission.

Department of Electrical and Computer Engineering

The University of British Columbia
Vancouver, Canada

Date Oct 3, 1999

DE-6 (2/88)

ABSTRACT

This thesis describes theoretical and experimental studies on two subjects: first is characterization, design and modeling of erbium-doped fiber amplifiers (EDFAs); second is the effect of fiber dispersion on the noise of distributed feedback (DFB) lasers and the impact of this effect on the performance of 1550nm video lightwave transmission systems.

A simple electrical measurement technique for EDFA noise figure characterization is developed which has significantly better accuracy than other methods reported. This is achieved by noise measurements at identical detected optical power levels, with and without EDFA present. This approach ensures that the system noise level is identical in both measurements, thereby even small EDFA noise levels can be separated accurately from the large noise of the measurement system by subtracting the two noise measurements. Using this technique an excellent agreement is obtained between optically- and electrically-measured noise figures of saturated EDFAs. This result is in contrast to earlier reports by Willems and van der Platts from Bell Laboratories, showing significant discrepancies between optically- and electrically-measured noise figures of a saturated EDFA which sparked a serious controversy over the appropriate approach to model and measure the noise figure of EDFAs.

Using the general, radially dependent rate-equation EDFA model, it is shown that highest-efficiency operation of saturated EDFAs is achieved with erbium distributed throughout the entire fiber core, in contrast to generally-accepted design principles. A simplified one-dimensional steady-state model for gain and noise in such EDFAs is derived which is accurate for any

arbitrary distribution of erbium doping inside the fiber core. It is shown that the saturation parameters normally included in conventional models can be eliminated without loss of accuracy, with the resulting model requiring only small-signal gain and loss coefficients as parameters. This great simplification eases fiber characterization, and enhances accuracy in predicting amplifier performance.

DFB laser relative intensity noise (RIN) variation induced by fiber chromatic dispersion is measured in the range of frequencies relevant to cable television systems. For two analog lasers tested, RIN degradation as large as 15dB is observed after 48km of standard fiber at a baseband frequency of 800MHz. The degradation increases with frequency, affecting higher channels the most. The experimental results are in excellent agreement with a simple theory by Yamamoto, which only requires knowledge of the laser linewidth to determine the RIN degradation. It is shown that this RIN degradation can significantly impair system carrier-to-noise ratio.

Table of Contents

List of Tables

List of Figures

Publications

I hereby declare that I am the sole author of this thesis.

In accordance with University of British Columbia thesis guidelines, I hereby declare that parts of this thesis has been or will be published under the following titles:

M. Movassaghi, M. K. Jackson, V. M. Smith, J. F. Young, and W. J. Hallam, "Noise figure of saturated erbium-doped fiber amplifiers: electrical versus optical measurement," in *Conference on Optical Fiber Communication OFC'97,* Vol. 6, 1997, OSA Technical Digest Series (Optical Society of America, Washington, D.C., 1997), paper WA2.

M. Movassaghi, M. K. Jackson, V. M. Smith and W. J. Hallam, "Noise figure of erbium-doped fiber amplifiers in saturated operation," *IEEE Journal of Lightwave Technology*, vol. 16, no. 5, May 1998.

M. Movassaghi, M. K. Jackson, V. M. Smith, J. F. Young, and W. J. Hallam, "Accurate frequency-resolved measurements of EDFA noise figure," in *Optical Amplifiers and Their Applications*, 1997 Technical Digest (Optical Society of America, Washington, D.C., 1997), paper TuD1.

M. Movassaghi and M. K. Jackson, "Design and modeling of saturated erbium-doped fiber amplifiers," to appear in *Tech. Dig. IEEE/LEOS Summer Topical Meet.*, San Diego, CA, USA, July 1999.

M. Movassaghi and M. K. Jackson, "Simple and accurate modeling of high-efficiency saturated erbium-doped fiber amplifiers," submitted for publication to *J. Lightwave Technol.* on July 27, 1999.

M. Movassaghi, M. K. Jackson and V. M. Smith, "DFB laser RIN degradation in CATV lightwave transmission," *Tech. Dig. IEEE/LEOS'98*, vol. 2, paper FB2, Dec 1998.

M. Movassaghi, M. K. Jackson and V. M. Smith, "Dispersion-Induced RIN degradation and its impact on 1550nm AM video lightwave transmission systems," revised manuscript under preparation for submission to *J. Lightwave Technol.*

Acknowledgement

My deepest gratitude goes to the members of my family for their encouragement and support throughout my education. I would also like to express my deep gratitude to my Ph.D. advisor Dr. Mike Jackson, for his knowledgeable guidance, patience and support throughout the course of this work and during my entire graduate studies. I found Mike to be a unique individual possessing a combination of many great qualities, including professionalism, dedication and brilliance. It was truly a great pleasure to work with Mike as I was continually learning new things from him. With no doubt, he played a major role in enhancing my knowledge, skills, and character; I owe him a great deal of gratitude. I also wish to thank Dr. Jeff Young, from Department of Physics and Astronomy, for his fruitful comments and suggestions during the course of my Ph.D. program.

I would like to express my gratitude to Vince Smith, Senior Development Engineer at Thomas&Betts Photon Systems, who helped me in many practical issues concerning my Ph.D. work. Vince was one the most skillful engineers I had ever known and working with him was a significant learning experience. My gratitude extends to John Maycock, former Vice President of Thomas&Betts Photon systems, who kindly provided me with the opportunity to conduct my Ph.D. research at Photon Systems. I would also like to acknowledge Wes Hallam, Development Engineer at Thomas&Betts Photon Systems, for his assistance in my experimental setups.

I would like to sincerely thank Dr. David Pulfrey for his help and support during difficult times associated with my M.A.Sc. program which dragged into the beginning of my Ph.D. Pro-

gram. I am also grateful to Dr. Bob Donaldson and Dr. Mike Davies, former and present heads of the Department of Electrical and Computer Engineering, for trusting me and providing me with the opportunity to teach EE474 for six consecutive terms during my Ph.D. program.

I would like to thank all of my friends especially, Dr. Shahram Tafazoli, Dr. Mohammad Sameti, Dr. Siavash Jahromi, Roberto Rosales, Dr. Mehrdad Sharifzadeh, and Sohrab Sigarian for their encouragement, help and support during the course of this work. I would also like to thank many wonderful staff members of the Department of Electrical and Computer engineering who helped me in various ways during the course of my graduate studies at UBC; in particular I am very grateful to Doris Metcalf, Cathleen Holtvogt, Leslie Leroux, Tony Leungner, Kathy Brindamour and Gail Schmidt.

Chapter 1

Introduction

1.1 Introduction to Thesis

1.1.1 Overview

This thesis describes theoretical and experimental studies on two subjects: first is characterization, design and modeling of erbium-doped fiber amplifiers operating in saturation; second is the impact of fiber dispersion on the relative intensity noise of distributed feedback (DFB) lasers. The above subjects are studied in the context of 1550nm optically amplified AM (amplitude modulated) video lightwave transmission systems, which are of particular interest to the industrial collaborator involved in this work, Thomas&Betts Photon Systems in Burnaby, B.C. However, the results shown in this thesis are relevant and applicable in general to many modern analog and digital fiber optic communication systems including the rapidly growing field of wavelength division multiplexing, in which saturated erbium-doped fiber amplifiers play a key role.

The work described in this thesis is composed of three major parts. The first part, concerning the erbium-doped fiber amplifier (EDFA) noise figure, describes a new technique for electrical noise figure measurements of EDFAs and comparison of results versus the conventional optical measurement technique. The second part, concerning design, modeling and characterization of

EDFAs, describes the design of highly efficient saturated EDFAs, describes a simplified yet accurate model for theoretical prediction of gain and noise figure in saturated EDFAs, and finally describes characterization techniques for obtaining the erbium-doped fiber parameters required for the model. The third part, concerning DFB laser noise, presents measurements of DFB laser relative intensity noise (RIN) in the frequencies relevant to the video lightwave transmission systems and shows that significant degradation of laser RIN can occur with dispersive fiber propagation. Finally, it describes modeling of laser RIN variation with fiber dispersion and discusses the consequence of this effect on the overall performance of the 1550nm optically amplified AM video lightwave transmission systems.

1.1.2 Outline of Chapter

The purpose of this chapter is to describe the motivation of the work and provide relevant background information on topics presented in this thesis. Section 1.2 describes motivation and incentives of the work presented in this thesis. In Section 1.3 operating principles of 1550nm optically-amplified AM video lightwave transmission systems are described. In Section 1.4 fundamentals of EDFA operation and EDFA noise sources are described. Section 1.5 describes conventional EDFA noise figure measurement techniques. In Section 1.6 conventional approaches for modeling EDFAs are presented. Section 1.7 describes DFB laser noise and its variation with fiber dispersion. In Section 1.8 laser RIN measurement techniques are described and finally Section 1.9 describes the organization of the remainder of the thesis.

1.2 Motivation

1550nm optically-amplified AM video lightwave transmission systems, which will be referred to as CATV (cable television) systems, are being extensively deployed around the world to replace coaxial networks. The underlying reason is that fiber-based systems can achieve higher quality transmission with much lower installation and maintenance costs. The coaxial networks contain many cascaded amplifiers to compensate the cable attenuation in the magnitude of several hundreds of decibel (dB) and accumulation of the noise of these amplifiers limits transmission span of coaxial networks. In comparison, the low loss of optical fibers at 1550nm, and the advent of erbium-doped fiber amplifiers (EDFAs), which optically amplify the signals in the 1550nm window, have enabled CATV systems to transmit up to 80 video channels over transmission span lengths of 120km or more [1]. In addition, at the end of the transmission line, high power and low noise erbium-doped fiber amplifiers allow the signal to be split among many users maintaining its high quality.

A stringent requirement for CATV systems is that a high signal-to-noise ratio is required at the receiver, and therefore in designing such systems the noise contribution from various components of the system must be carefully analyzed and modeled. Beside the receiver shot noise, two of the essential noise contributors in these systems are the erbium doped fiber amplifier (EDFA), used as power and/or inline amplifier, and the DFB laser in the transmitter. In addition, as EDFAs play the role of amplifying and boosting the optical signal, modeling of the gain of these amplifiers is also of particular importance. The work presented in this thesis concerns theoretical and experimental analyses on several important issues regarding the EDFA gain and noise and

also the noise of DFB lasers.

1.3 Operating Principles of CATV Systems

A layout of a basic 1550nm optically-amplified AM video lightwave transmission system (CATV systems) is shown in Fig. 1.1. It consists of a DFB laser operating in CW (continuous wave) mode employed as an optical carrier. A number of amplitude-modulated vestigial side-band (AM-VSB) TV channels, typically between 40 to 120 channels, which have frequencies between 50 to 800 MHz, with 6MHz channel spacing and each having 4MHz bandwidth are combined using an RF power combiner. The resulting composite signal is then applied to a linear electro-optic modulator to intensity modulate the optical carrier. The output of the modulator is optically amplified by an erbium doped fiber amplifier and the EDFA output is launched to the transmission fiber at the other end of which the optical signal is converted back to an electrical signal using an optoelectronic receiver. As the TV channels are formed by AM modulation, the performance of CATV systems is significantly affected by the noise of the different components in these systems. For optimum design of CATV systems the noise characteristics of different components of these systems should be analyzed. In this thesis, several issues concerning the noise of the EDFA and DFB laser, which are important contributors of noise in CATV systems, are analyzed.

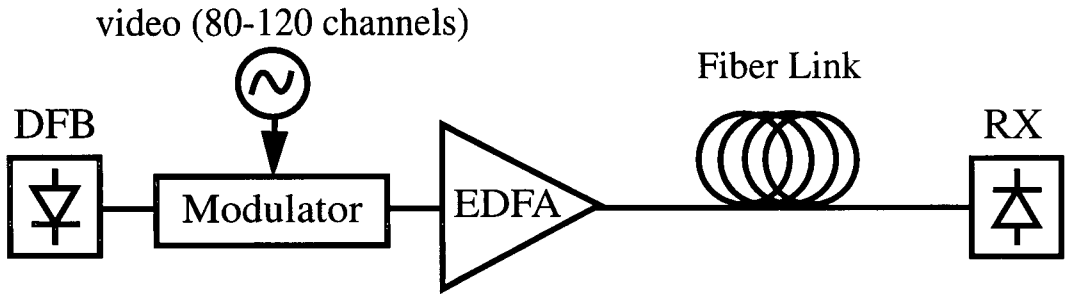

Figure 1.1: Basic system configuration for 1550nm optically-amplified AM video lightwave transmission systems (CATV systems). Components are described in the text.

1.4 Erbium-Doped Fiber Amplifiers (EDFAs)

The advent of erbium-doped fiber amplifiers in 1987 revolutionized the field of optical fiber communication. Prior to the advent of EDFAs, the standard way to compensate for the attenuation of the optical fiber transmission line was to use electronic regenerators. In these regenerators the weak optical signal is converted into an electrical signal using an optoelectronic receiver, the electrical signal is then amplified and converted back into an optical signal by an electro-optic transmitter. Besides the complexity and high cost, the bandwidth of such regenerators is limited by the speed of their electronic components, which is much lower than the bandwidth of the optical fiber, thus limiting the transmission capacity of the entire fiber optic communication system. In contrast, EDFAs allow direct optical amplification of the weak signals along the fiber transmission link and therefore are not limited by any electronic bandwidth, thus allowing a dramatic increase in transmission capacity compared to electronic regenerators. In addition, EDFAs have several other attractive features such as high gain, high output power, high efficiency, polar-

ization insensitivity, and low noise figure. These attributes have made the EDFA an exceptionally important component in most analog and digital lightwave communication systems.

1.4.1 Operating Principles

A basic architecture of an EDFA is illustrated in Fig. 1.2. The light from the signal laser (between 1520nm-1560nm) and the light from the pump laser (typically either at 980nm or 1480nm) are coupled to the erbium-doped fiber (EDF) with a wavelength division multiplexer (WDM). The EDF is made by incorporating erbium dopants together with germania (GeO_2), and/or alumina (Al_2O_3) into the silica fiber core using various techniques [2]-[3]. Germania is used as an index-raising codopant and alumina improves the solubility of erbium into silica fiber, resulting in higher concentration doped fiber. An isolator at the end of the EDF blocks any back-reflections to the EDFA from the downstream line. The architecture shown in Fig. 1.2 is called a co-directionally pumped configuration as the pump is travelling in the same direction of the signal inside the EDF. In another EDFA architecture, signal and pump travel in opposite directions, which is called counter-directionally pumped configuration. There are several other architectures for EDFA which are obtained by using one or more co- and counter- propagating pumps, isolators, optical filters and cascading stages. However, the principles of their operation are generally identical. The focus of the work presented in this thesis is on the single stage co-directionally pumped EDFAs, which are normally used in CATV systems.

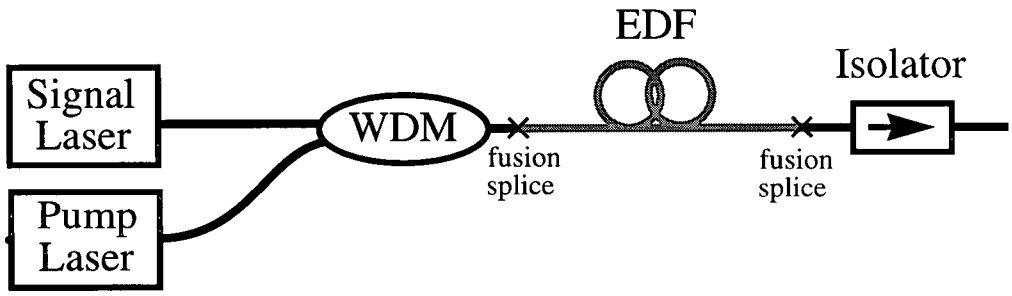

Figure 1.2: A basic architecture of an EDFA

The EDFA operation principles can be described by considering the first three energy levels for the erbium in a silica glass, which are shown in Fig. 1.3. The shaded rectangles in the figure indicate that each main energy level is split into a manifold of multiple energy sublevels due to the Stark effect. The Stark effect is induced by the permanent electric field, which is generated by charge distribution in the glass host [4]. Nevertheless, due to the effect of intramanifold thermalization, which maintains a constant population distribution within the manifolds (Boltzmann's distribution), each manifold can be considered as a single energy level [2]-[4].

Among the several transitions that can be used to pump EDFAs, ${}^4I_{15/2} \rightarrow {}^4I_{11/2}$ and ${}^4I_{15/2} \rightarrow {}^4I_{13/2}$ transitions, corresponding to 980 and 1480nm pumping, respectively, are the most efficient pump bands. For 980nm pumping, the EDFA behaves like a three level system; the energy from the pump laser boosts the erbium ions from the ground state (${}^4I_{15/2}$ manifold) to the pump state (${}^4I_{11/2}$ manifold), from which the ions relax to the metastable state (${}^4I_{13/2}$ manifold). Since the relaxation rate of ions from the pump state to the metastable state is much higher than the pumping rate, the population of the erbium ions in the pump state is negligible

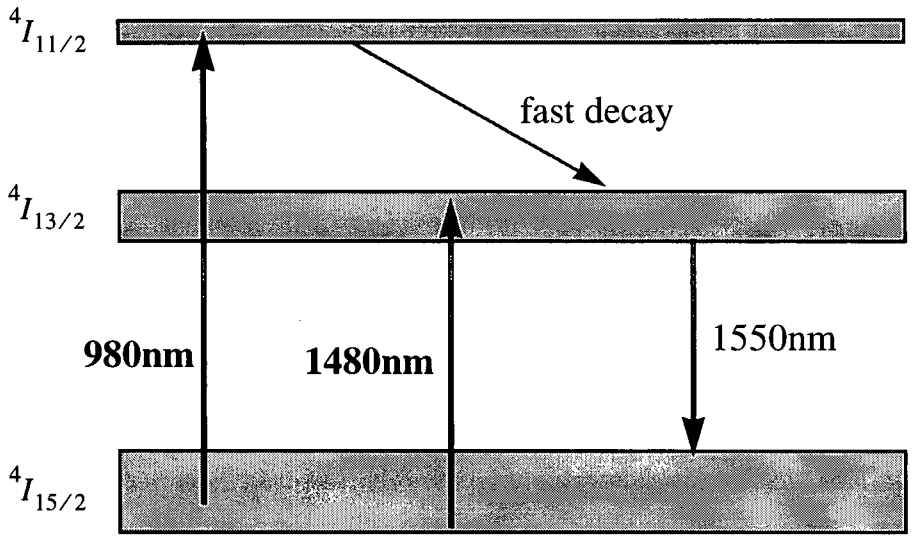

Figure 1.3: The first three energy levels of erbium in a silica glass host

and a high degree of population inversion can be achieved. Therefore, the 980nm pumped EDFAs can be analyzed by considering only two levels. For 1480nm pumping, the energy from the pump laser excites the erbium ions in the low lying levels of the $^4I_{15/2}$ manifold to the high lying ones in the $^4I_{13/2}$ manifold, leading to a population inversion between the two main energy levels; the 1480nm pumped EDFAs can also be analyzed by considering only two levels. Once in the metastable state, the ions are stimulated by the signal propagating along the EDF, causing them to decay back to the ground state; this results in the emission of photons in phase with the signal, thus amplifying the signal by stimulated emission. Amplification at wavelengths approximately between 1520 to 1560nm takes place between the low lying levels of the $^4I_{13/2}$ manifold and the high lying ones in the $^4I_{15/2}$. Besides the stimulated emission, there exists a competing process of spontaneous emission. The photons arising from this process have no coherence characteristics with respect to the signal; some of the spontaneously emitted photons are captured by the fiber and then amplified, leading to amplified spontaneous emission (ASE) at the EDFA output. Therefore, the output spectrum of an EDFA consists of the amplified input spectrum, and the broadband ASE, which is known to be the major EDFA noise contributor [2]-[4].

Besides the transitions shown in Fig. 1.3 there exist additional transitions associated with an undesirable phenomena called pump excited state absorption (ESA). In this process, the pump photons at frequency ν_p are not absorbed from the ground state $^4I_{15/2}$, but are absorbed from the metastable level $^4I_{13/2}$. This is due to existence of another level whose energy gap with the metastable level happens to closely match the pump photon energy $h\nu_p$, where h is Planck's

constant. For 980nm pumping, ESA occurs between the metastable level (level 2) and level 4 and for 1480nm pumping this occurs between level 2 and $^4I_{11/2}$ manifold (level 3). The pump ESA process would therefore result in an excess loss for the pump, which reduces the amplifier gain. However, it has been shown that for the 980nm and 1480nm pumping, the pump ESA is very small and almost negligible [4]-[5].

Operating conditions of EDFAs are generally grouped into two regimes, unsaturated and saturated regimes. Unsaturated regime corresponds to the conditions where the amplifier gain is within 3dB of its small signal gain and saturated regime refers to the conditions where the amplifier gain is reduced more than 3dB from its small signal gain. Small signal gain is the highest gain of an EDFA.

1.4.2 Noise sources

The noise that will be seen on a photodetector placed after an EDFA is comprised of signal shot noise, ASE shot noise, signal-ASE beat noise, ASE-ASE beat noise, and interferometric noise. The first two of these are the shot noise generated in the receiver's photodetector due to the EDFA output signal power level and the ASE power level. The signal-ASE term is caused by heterodyne mixing between the amplified signal and the ASE at the receiver's photodetector. This is generally the dominant noise source of EDFAs. The ASE-ASE term is generated due to heterodyne mixing of the ASE with itself. Interferometric noise is caused by heterodyne mixing of the main optical output signal with the multiply backscatterd optical fields which are generated by reflections from EDFA components and/or reflections due to fiber Rayleigh scattering.

The relative intensity noise (RIN), defined in Section 1.5.2, corresponding to the interferometric noise, is given by [3],[6]-[7]:

$$RIN_{MPI}(f) \propto \frac{\Delta\nu}{f^2 + \Delta\nu^2} \tag{1.1}$$

where MPI denotes multi-pass interference, $\Delta\nu$ is the source laser linewidth, and f is the noise frequency. Therefore, interferometric noise is frequency dependent and its influence on the total noise of an EDFA reduces at higher frequencies; the rate of this reduction is greater for laser sources with smaller linewidths.

1.5 Conventional EDFA Noise Figure Measurement Techniques

The noise figure (NF) of an amplifier is a measure of the degradation of the signal-to-noise ratio for a signal passing through the amplifier, with the signal and noise measured in the electrical domain. However, due to difficulties in making such measurements in the electrical domain, an alternative approach called the optical method has prevailed and is generally used for determination of the EDFA noise figure [3], [7]-[8]. In this section both the conventional electrical and optical methods are described.

1.5.1 Optical Measurement Techniques

The optical NF measurement techniques are based on measuring the amplifier signal gain and ASE power, using an optical spectrum analyzer, and then calculating the noise figure from a theoretical relationship given by [3]-[4], [7]-[9]:

$$NF = \frac{P_{ASE}}{h\nu\,\Delta\nu\,G} + \frac{1}{G} \tag{1.2}$$

where P_{ASE} is the total EDFA amplified spontaneous emission power within the optical bandwidth of $\Delta\nu$, ν is the optical signal frequency and G is the EDFA gain at the signal wavelength. However, the above expression only includes the shot noise and signal-ASE noise contributions. In fact, it is assumed that the other EDFA noise terms are negligible.

Fig. 1.4 shows the experimental setup for measuring P_{ASE} and G. The main experimental apparatus is an optical spectrum analyzer (OSA) which measures the power spectrum. To determine the noise figure, two measurements are performed. The first is a measurement of the laser source spectrum that is used to determine the input signal level to the EDFA (P_{in}) and the source spontaneous emission level at the signal wavelength (SSE). The second is a measurement of the output spectrum of the EDFA to determine the signal power level and the output spontaneous emission (OSE). The difference in the signal levels from the two measurements is the EDFA gain (G). The OSE contains the SSE multiplied by the amplifier gain plus the P_{ASE}, i.e.

$$OSE = SSE \times G + P_{ASE} \quad . \tag{1.3}$$

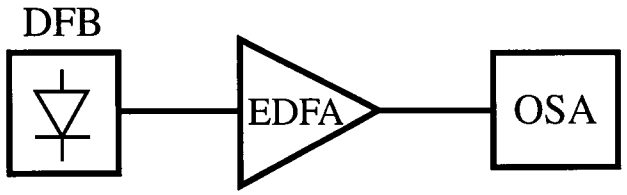

Figure 1.4: Experimental setup for optical NF measurements.

To precisely determine the noise figure, P_{ASE} must be determined at the signal wavelength. However, this cannot be measured directly as the signal power level masks the ASE level at the signal wavelength; instead it is determined using the linear interpolation technique [10]. In this technique, the SSE and OSE levels are measured at a wavelength just above and just below the signal wavelength. Knowing the amplifier gain, P_{ASE} at the signal wavelength is then determined from equation (1.3) and using a linear interpolation. This technique is based on the assumption that the ASE produced by the EDFA is linear (on a linear scale) over a small wavelength range (typically +/- 1nm) about the signal. This assumption is well justified as experimental evidence for typical EDFAs indicates that the maximum ASE deviation from a straight line fit over a +/- 1 nm range is less than 1% at all wavelengths between 1542 to 1565 nm; this is the wavelength region in which EDFAs are commonly used [10]. However, although the linear interpolation technique is relatively simple and expected to be highly accurate for EDFAs operating in the unsaturated regime, it has been argued that it is not accurate for amplifiers operating in saturation [8]-[12]. The argument is based on the fact that in saturation, amplified sideband components of the signal become comparable to ASE, due to the reduction of the ASE power level in saturation, and distort the shape of the ASE spectrum around the signal, therefore mak-

ing it difficult to measure the ASE level accurately. A polarization nulling technique was proposed to improve the accuracy of noise figure measurements in saturation [9]. This technique, which has become widely accepted, is built upon the fact that the ASE is randomly polarized, whereas the input signal is polarized in one direction. Therefore by adding a polarization state controller and a linear polarizer between the EDFA and the optical spectrum analyzer (OSA), ideally it is possible to suppress the amplified signal and its sidemodes and, thereby, measure the ASE level at the signal wavelength. However, experimental measurements have shown large residual components of the signal even at 40 dB signal suppression [11]-[12]. Therefore in practice the interpolation technique is used in conjunction with polarization nulling to accurately determine P_{ASE} and thereby the EDFA noise figure [10].

1.5.2 Electrical Measurement Technique (RIN Subtraction Method)

The conventional electrical noise figure measurement technique is based on the method proposed by Willems et. al. which is known as the RIN (relative intensity noise) subtraction method [7], [13]-[15]. In this method, the NF is related to the RIN at the input and output of the EDFA through the expression,

$$NF = \frac{(RIN_{output} - RIN_{signal})\, P_{in}}{2h\nu} + \frac{1}{G}, \tag{1.4}$$

where P_{in} is the optical input power, and G is the amplifier gain. RIN_{output} and RIN_{signal} are the RIN measured at the output and input of the EDFA, respectively. The RIN of a signal is defined as $\Delta P^2 / P^2$ expressed in units of dB/Hz, where ΔP^2 is the mean square optical inten-

sity fluctuations (in a 1 Hz bandwidth) at a particular frequency, and P^2 is the square of the optical power [3]. The RIN is measured using a commercial Hewlett-Packard 71400 lightwave signal analyzer, which is an optoelectronic receiver connected to an RF spectrum analyzer. This equipment determines the RIN automatically by subtracting the signal shot noise and the receiver thermal noise from the total noise measured, and from measurements of optical signal power and several frequency dependent system parameters; these parameters are photodetector, amplifier, and spectrum analyzer frequency responses as well as mismatch losses between them [10], [16]. The accuracy of the RIN measurement using the HP 71400 is estimated to be ±2 dB [14]. This rather large uncertainty in RIN measurement directly limits the accuracy of the electrical measurement technique, specially for the saturated EDFAs where RIN_{output} approaches RIN_{signal}. In Chapter 2 of this thesis a new electrical NF measurement technique is described which has an absolute accuracy of ±0.3 dB.

1.6 Modeling Gain and Noise Figure in EDFAs

To predict the gain and noise properties of EDFAs, models based on propagation and rate equations of a homogeneous, two level system have been used [2]-[4]. In these models, the broadband ASE spectrum, having a total spectral width of $\Delta\nu$, is discretized into k optical beams having a frequency bandwidth of $\Delta\nu_k$ centered at the optical wavelength $\lambda_k = c/\nu_k$. $\Delta\nu_k$ are the frequency steps used in the simulation to resolve the ASE spectrum, and therefore $k = \Delta\nu/\Delta\nu_k$. To model the evolution of signal, pump, and ASE, a set of differential-integral equations, each corresponding to one optical beam in the spectral slot of $\Delta\nu_k$ and center wave-

length λ_k, have to be solved. By considering that ASE propagates in two directions (forward and backward), the total number of equations would then become $2k + n$, where n is the total number of signal and pump sources [2]-[4]. These equations are coupled and have to be solved numerically, requiring complex programming and substantial computational time. For future reference, the above approach will be referred to as the "comprehensive model". The number of equations and therefore the complexity of the numerical calculations in the comprehensive model can be significantly reduced by considering ASE as only two optical beams at the signal wavelength with an effective bandwidth, propagating in the forward and backward directions. This model is called the effective ASE model and for 980 pumping the equations describing propagation of the signal, P_s, pump P_p and total ASE propagating in the forward and backward directions, P_a^+ and P_a^-, can be written as [4], [17] (see Appendix A for details of derivations):

$$\frac{dP_s}{dz} = \frac{2P_s}{\omega_s^2} \int \rho(r) \left[\sigma_{se}\, n_2(r) - \sigma_{sa}\, n_1(r)\right] \psi_s(r)\, r\, dr - \alpha'_s P_s \tag{1.5}$$

$$\frac{dP_p}{dz} = \frac{-2P_p}{\omega_p^2} \int \rho(r) \left[\sigma_{ESA}\, n_2(r) + \sigma_{pa}\, n_1(r)\right] \psi_p(r)\, r\, dr - \alpha'_p P_p \tag{1.6}$$

$$\pm\frac{dP_a^{\pm}}{dz} = \frac{2}{\omega_s^2} \int \rho(r) \left\{\sigma_{se}\, n_2(r) \left[P_a^{\pm} + 2h\nu_s \Delta\nu_{eff}\right] - \sigma_{sa}\, n_1(r)\, P_a^{\pm}\right\} \psi_s(r)\, r\, dr - \alpha'_s P_a^{\pm} \tag{1.7}$$

where subscripts s and p denote the signal and pump, respectively, ψ_s and ψ_p are the radial mode envelope distributions with unity peak, ω_s and ω_p are the power mode sizes, and z is the fiber longitudinal coordinate. $\rho(r)$ is the erbium density distribution, σ_{se} and σ_{sa} are the emission and absorption cross sections at the signal wavelength, respectively; σ_{pa} and σ_{ESA} are the absorption cross section and excited state absorption cross section at the pump wavelength, respectively. α'_s and α'_p are the fiber back-ground loss coefficients at the signal and pump wavelengths, respectively. $n_1(r)$ and $n_2(r)$ are the ground and upper level population densities normalized by $\rho(r)$, which satisfy $n_1(r) + n_2(r) = 1$. $n_2(r)$ is given by [4] (see Appendix A for details of derivation):

$$n_2(r,z) = \frac{\dfrac{P_p(z)}{P_p^{sat}}\psi_p(r) + \dfrac{\sigma_{sa}}{\sigma_{sa}+\sigma_{se}}\dfrac{P_s(z)+P_a^+(z)+P_a^-(z)}{P_s^{sat}}\psi_s(r)}{1 + \dfrac{P_p(z)}{P_p^{sat}}\psi_p(r) + \dfrac{P_s(z)+P_a^+(z)+P_a^-(z)}{P_s^{sat}}\psi_s(r)} \tag{1.8}$$

where

$$P_s^{sat} = \frac{h\nu_s \pi \omega_s^2}{(\sigma_{se}+\sigma_{sa})\tau} \tag{1.9}$$

and

$$P_p^{sat} = \frac{h\nu_p \pi \omega_p^2}{\sigma_{pa}\tau} \tag{1.10}$$

are the intrinsic saturation powers at the signal and pump wavelengths, respectively. ν_s and ν_p are the optical frequencies, h is Planck's constant, and τ is the spontaneous emission lifetime. In the above model, the ASE is modeled as forward and backward propagating optical beams centered at the signal wavelength with an effective ASE bandwidth given by [10], [20],

$$\Delta\nu_{eff} = \int_0^{\infty} (\sigma_e(\nu) / \sigma_e(\nu_s)) \, d\nu \, . \tag{1.11}$$

The noise figure, NF, is calculated using

$$NF = \frac{P_a^+(L)}{h \nu_s \Delta\nu_{eff} \, G} + \frac{1}{G} \tag{1.12}$$

where $P_a^+(L)$ is the total ASE power at the output end of the amplifier. The effective ASE model provides an accurate estimate of the noise figure, and allows approximate evaluation of the impact of ASE on the population $n_2(r)$.

The comprehensive model and the effective ASE model described above, although are most suitable for accurate theoretical prediction of gain and noise figure of EDFAs, but they are not very practical as they include many parameters some of which are difficult to measure accurately. Among these parameters are erbium ion concentration and distribution inside fiber core, optical mode distributions, emission and absorption cross sections and fluorescence lifetime [3]-[4], [17]-[18]. Alternately, several models based on various assumptions have been developed

which provide a more practical way to model EDFAs [3]-[4], [17]-[20]; among these a model developed by Saleh et. al. [19]-[20], has been widely accepted and used for modeling of EDFAs operating in saturation [21]-[27]. This model is derived from the comprehensive model based on neglecting the effect of amplified spontaneous emission on erbium ions population inversion, excited state absorption, and fiber background losses at the signal and pump wavelengths. In addition it has been assumed that the area of the erbium-doped active region is so small, i.e. erbium is well confined near the center of the core, such that the radial mode envelope distributions at the pump and signal wavelengths are identical. Accordingly, the amplifier gain is obtained from the following equations:

$$P_k^{out} = P_k^{in}\, e^{-\alpha_k L}\, e^{(P_{in} - P_{out})/P_k^{sat}} \tag{1.13}$$

where P_k^{in} and P_k^{out} are the input and output powers of the kth optical beam and where

$$P_{in} = \sum_{j=1}^{N} P_j^{in} \qquad \text{and} \qquad P_{out} = \sum_{j=1}^{N} P_j^{out} \tag{1.14}$$

are the total EDFA input and output powers, respectively. α_k is the small signal absorption coefficient of the kth beam and L is the length of the amplifier. By summing both sides of equation (1.13) over k, P_{out} can be obtained by solving a transcendental equation based on knowing the parameters α_k, P_k^{sat}, and the input powers. Once P_{out} is obtained, it is inserted into equation (1.13) to obtain the output P_k^{out}, and hence the gain, at each wavelength. α_k and P_k^{sat} at each wavelength can be obtained by monochromatic loss measurements at several input powers to the

EDF and fitting equation (1.13) to the results [19]. For noise figure calculations, the power of amplified spontaneous emission P_{ASE} at the EDFA output is required (see equation (1.2)). This is obtained by multiplying the spontaneous emission from each infinitesimal section of the EDFA by the gain it experiences to the end of the amplifier, and integrating that over the length of the amplifier. Accordingly, P_{ASE} at the EDFA output is given by:

$$P_k^{ASE}(L) = \Delta\nu \; g_k \int_{z=0}^{z=L} N_2(z)\, G_k(z, L)\, dz \tag{1.15}$$

where

$$N_2(z) = \frac{\sum_{j=1}^{N} \alpha_j \, P_j(z)}{\zeta \sum_{j=1}^{N} [1 + P_j(z)/P_j^{sat}]} \tag{1.16}$$

is the population of the second level, $G_k(z, L)$ is the gain of the kth optical beam from position z to the end of the amplifier. $\zeta = \rho A/\tau$, where A is the area of the doped region; ζ is obtained from $\zeta = \alpha_\lambda P_\lambda^{sat}$ at $\lambda = 980nm$. g_k is the small signal gain coefficient which is obtained from $g_k = (\zeta / P_k^{sat}) - \alpha_k$.

In Chapter 3 of this thesis it is shown that the efficient design of a saturated EDFAs is achieved by not confining the erbium and distributing it across the entire fiber core. Given that Saleh's model is derived based on the assumption that the erbium is well confined, it cannot

accurately predict the performance of non-confined EDFAs. In Section 3.5 a simple model is derived which can closely predict the gain and noise figure of non-confined EDFAs.

1.7 Effect of Fiber Dispersion on DFB Laser RIN

A fundamental source of noise in lasers is due to the spontaneous emission which continually adds new power to the laser oscillation field generated by the stimulated emission. The electromagnetic field associated with the spontaneous emission is not coherent with the field generated by the stimulated emission, and therefore the laser output field fluctuates both in amplitude and in phase. Therefore, the actual electric field of a single mode laser can be represented by

$$E(t) = (E_0 + \Delta E(t)) \exp[i(\omega_0 t + \varphi(t))] \tag{1.17}$$

where E_0 is the amplitude, $\Delta E(t)$ is intrinsic amplitude fluctuation (intrinsic amplitude noise), ω_0 is the central angular frequency, and $\varphi(t)$ is the phase fluctuation (phase noise) of the laser electric field. It should be noted that since both amplitude and phase fluctuations originate from the same source, spontaneous emission, they are correlated. At the laser output the measured intensity noise is only due to the intrinsic amplitude noise and the phase noise does not cause any intensity noise. However, through dispersive fiber propagation, different frequency components of the laser electric field, caused by the phase noise, travel at different velocities, thus reaching to the end of the fiber at different times. In a photodiode placed at the end of fiber, these delayed components are mixed interferometically causing amplitude noise. Since this amplitude noise originates from the laser phase noise, this phenomena is called phase to intensity or PM

(phase modulation) to AM (amplitude modulation) noise conversion. Therefore, after dispersive propagation, the laser intensity noise is due to a combination of the laser intrinsic amplitude noise and an additional amplitude noise created by the PM to AM noise conversion.

The effect of fiber dispersion on the semiconductor laser intensity noise has been analyzed with two different approaches. In one approach, by Yamamoto et. al. [28], the laser intrinsic amplitude fluctuation $\Delta E(t)$ in equation (1.17) is neglected and only phase fluctuations are considered. The result of this analysis leads to a simple expression showing a proportional increase in the laser intensity noise by the fiber dispersion and laser linewidth. In the second approach, by Marshall et. al. [29], both of the laser intrinsic amplitude and phase noise together with the process correlating these two noise sources are considered. The resulting model is thus comprehensive, but it is complicated and contains several laser parameters which are difficult to measure accurately. Their results show that over moderate distances (several km for standard single mode fiber at 1550nm) the laser intensity noise is reduced over a wide range of frequencies, but for longer fiber distances the intensity noise is proportionally increased with fiber length. Fig. 1.5 shows their measurement results for relative intensity noise (RIN) of a 1550nm DFB laser and its variation after 4.1 km and 20 km of standard single mode fiber. The reduction and increase of laser RIN for the two lengths of fiber shown in Fig. 1.5 is clearly visible for frequencies above 1GHz; however, the measurement results become uncertain below 1 GHz as it is difficult to measure RIN accurately because of its low level. Chapter 4 of this thesis, presents a detailed analysis of the effect of fiber dispersion on the DFB laser RIN for frequencies relevant to CATV systems (below 800 MHz).

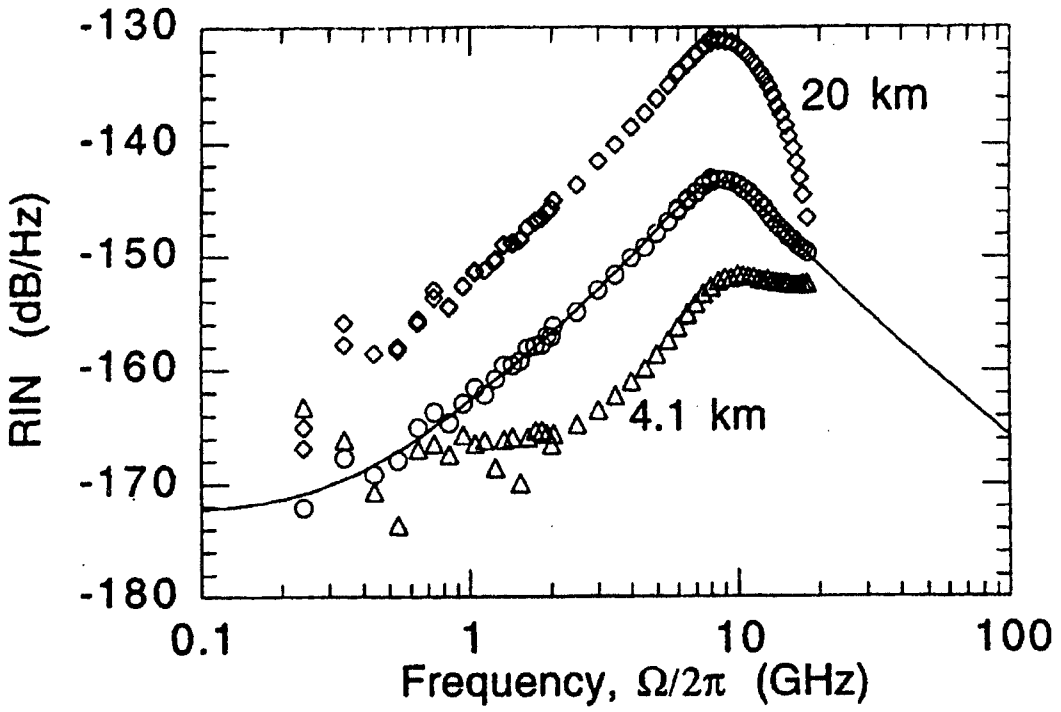

Fig. 1.5: Measured RIN at the 1550nm DFB laser (circles), and after propagation in the standard single mode fiber of length 4.1 km (triangles) and 20 km (diamonds). From Ref. [29].

1.8 Laser RIN Measurement Techniques

The conventional laser RIN measurement technique is based on the approach described in Section 1.5.2. The limitation of this technique is that it requires knowledge of several frequency dependent system parameters, which are difficult to measure. In another RIN measurement approach, developed by Nazarathy, et. al. [30], laser RIN is obtained independently of these parameters. In this method the laser voltage noise spectral density is measured, using an optoelectronic receiver attached to an RF spectrum analyzer, at several optical received powers; laser RIN is then extracted form least squares fitting of the following equation to the measured results [30]:

$$N_T - N_{dark} = RIN\ R^2\ H\ P^2 + 2\ e\ H R P \tag{1.18}$$

where N_T is the voltage noise spectral density, and N_{dark} is the voltage noise spectral density in the absence of light to the receiver (laser is disconnected from the receiver). R is responsivity of the photodiode in the optoelectronic receiver, H is the transimpedance gain from the photodiode's current to the input voltage of the spectrum analyzer, and P is the optical power input to the receiver[1].

The measurement approach by Nazarathy et. al., provides a simpler means for laser RIN measurements than the conventional method as it requires knowledge of only three parameters.

---

1. The above definitions given for the parameters contained in equation (1.18) are from Ref. [30]; however it is believed that the proper definitions for N_T and N_{dark} are that they denote the noise power spectral densities and H is equal to Z^2/Z_{in}, where Z is the transimpedance of the network connecting the photodiode to the spectrum analyzer and Z_{in} is the spectrum analyzer input impedance (See Chapters 2 and 4 for more details).

In Chapter 4 of this thesis, a similar method is used to measure laser RIN.

1.9 Outline of the Thesis

Chapter 2 describes a new electrical noise figure measurement technique which can provide accurate determination of the EDFA noise figure. A comparison between electrically- and optically- measured noise figures of two EDFAs is presented showing excellent agreement between the two measurement approaches; this confirms the applicability of conventional homogeneously broadened two level system model for EDFA noise prediction. The agreement obtained between the two measurement approaches is in contrast to earlier reports showing significant discrepancies between electrically- and optically- measured noise figure of a similar saturated EDFA.

In Chapter 3, it is shown that highest-efficiency operation of saturated EDFAs is achieved with erbium distributed throughout the entire fiber core, in contrast to generally-accepted design principles. It is shown that the commonly used Saleh model cannot accurately predict the performance of non-confined EDFAs and a simplified EDFA model is derived which can accurately predict gain and noise figure of confined and non-confined EDFAs. A comparison between the predictions of the proposed model and the experimental gain and NF of a 980nm-pumped EDFA is presented showing an excellent agreement between them.

In Chapter 4, an enhanced measurement method for simple and accurate characterization of laser RIN is described. Measurements of laser RIN are presented in the range of frequencies relevant to CATV systems, and for the first time, lowest RIN values as low as -172 dB/Hz are

shown for an analog 1550nm DFB laser. Laser RIN measurements versus several lengths of standard fiber, up to 48 km, are presented and it is shown that for the case of CATV systems, RIN degradation by fiber dispersion can be significant. Finally, excellent agreement between the experimental results with predictions of a simple theory which relates laser RIN degradations to the laser linewidth is presented.

Chapter 2

Noise Figure of Erbium-Doped Fiber Amplifiers in Saturated Operation

2.1 Introduction

As described in Chapter 1, one of the main objectives of the Ph.D. research being presented in this thesis is to develop a model for accurate prediction of the gain and noise figure in saturated erbium-doped fiber amplifiers (EDFAs). One of the important factors involved in achieving this goal was having access to reliable techniques for accurate measurements of EDFA gain and noise figure (NF), allowing reasonable comparison to be made between model predictions and experimental results. While conventional techniques were sufficiently accurate for gain measurements, there was a serious controversy over the appropriate technique for measuring NF of saturated EDFAs. Obviously, prior to any attempt to develop the model, the possibilities of being able to make accurate NF measurements should have been assessed. In this chapter a new technique for accurate measurement of EDFA noise figure is presented which has an absolute accuracy within ± 0.3 dB for noise figure measurements.

This chapter is organized as follows. In Section 2.2, the motivation of this work, which furnishes an outline of the previous attempts in measuring EDFA noise figure and controversy surrounding the appropriate approach for its measurement, is described. In Section 2.3, a new electrical noise figure measurement technique is described. This technique is based upon mea-

surement of the electrically-detected noise levels with and without the amplifier present. By adjusting the optical power levels at the detector to be identical for these two measurements, it is ensured that contributions from shot, thermal, and input RIN noise are identical; therefore the EDFA noise contribution can be recovered by subtracting the results of the two measurements. In Section 2.4, the method used for optical NF measurements is described. This method is based on the conventional polarization nulling technique, together with a calibration technique which allows accurate determination of the loss incurred by the polarizer and the polarization controller. In Section 2.5, the results of electrical and optical NF measurements are presented, compared and discussed. Finally, summary and conclusions of the results presented in this chapter are in Section 2.6.

2.2 Motivation

As described in Chapter 1, conventional techniques for NF measurement can be grouped into two categories: electrical and optical methods. The definition of noise figure for an optical amplifier refers explicitly to measurements made with electrical detection [31], making the link between the results of electrical characterization and noise figure straightforward. However, accurate measurement of the very low levels of noise is challenging, and most reports of NF measurement have been based on optical measurements [3], [7]-[9]. Hentschel et. al. have compared optical and electrical NF characterization for amplifiers operating in the unsaturated regime, and found good agreement between the two results [7]. However, later in 1995, Willems and van der Platts questioned the validity of optical NF measurements of saturated EDFAs [13]-

[14]. For a 980nm-pumped copropagating EDFA operating in the signal-saturated regime, these authors found that the results of optical NF measurements were significantly higher than those derived electrically. Fig. 2.1 illustrates the results of their measurements. The upper curve shows the measured optical NF and the lower curve shows the electrical NF versus optical input signal power to the EDFA. As can be seen from this figure, at high input signal powers where the EDFA is saturated, the electrical NF decreases while the optical NF increases for higher input signal powers. They attributed the decrease of the electrical NF to a reduction in statistical fluctuations due to gain saturation predicted by a qualitative consideration of nonlinear photon statistics in the EDFA [4]. Consequently, they concluded that optical measurement methods can lead to overestimation of the actual NF of saturated EDFAs. This was also an indication that the commonly-used semi-classical EDFA models cannot provide valid noise figure predictions for saturated EDFAs; this is because these models commonly predict that the EDFA noise figure rises as the amplifier is driven deeper into saturation. These conclusions, created a significant controversy over the appropriate approach to measure and model the noise figure of saturated EDFAs.

In this Chapter, a new electrical NF measurement technique is presented which has significantly better accuracy compared to the conventional method. Using this method, a similar comparison between optically- and electrically-measured NF of two amplifiers, similar to the one used in Ref. [13]-[14], is performed. The results show excellent agreement between the two measurement approaches, which is in contrast to the results of Willems and van der Platts [32]-[34].

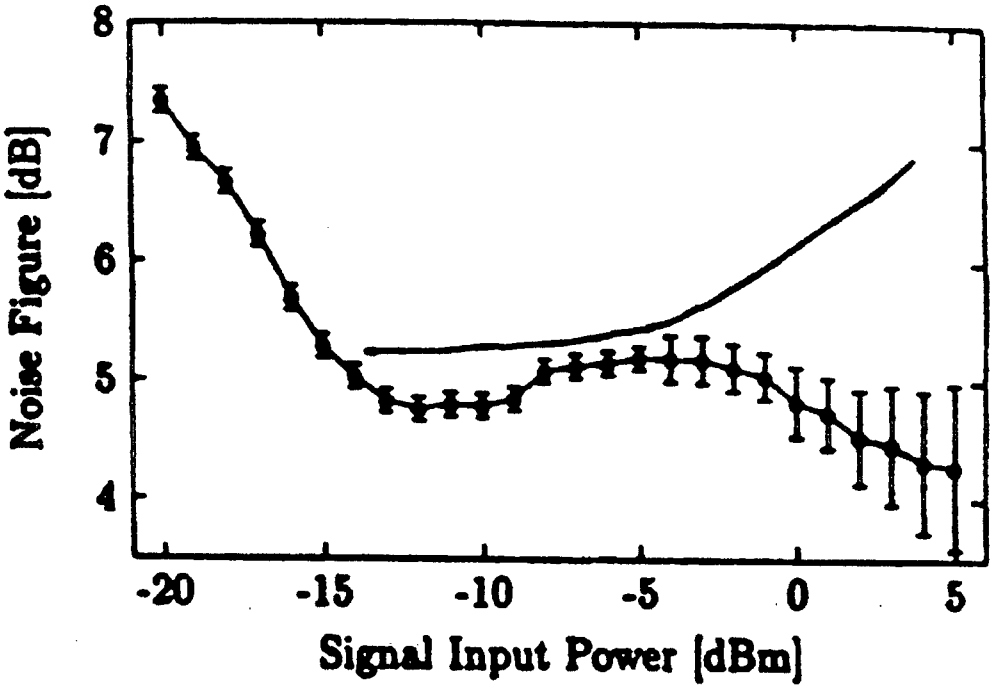

Figure 2.1: Noise figure of a 980-nm co-propagating EDFA as a function of signal input power measured with the conventional Optical Method (upper curve) and the conventional Electrical Method, RIN subtraction method (lower curve). (From Ref. [14])

2.3 A New Electrical Noise Figure Measurement Technique

In this section an expression is derived which relates the EDFA noise figure to parameters which can be measured simply and accurately. An electrical measurement technique for accurate determination of these parameters is then described.

The NF of an optical amplifier is defined as the ratio of the input signal-to-noise ratio (SNR), to output SNR, with the SNRs measured at the output of an ideal photodiode (IPD). With the SNRs expressed in terms of the mean squares of noise photocurrent at the output of the IPD, the NF equation is given by [7],

$$NF = \frac{SNR_{input}}{SNR_{output}} = \frac{\langle i^2_{signal}\rangle_{in}}{\langle i^2_{noise}\rangle_{in}} \times \frac{\langle i^2_{noise}\rangle_{out}}{\langle i^2_{signal}\rangle_{out}} = \frac{1}{G^2}\,\frac{\langle i^2_{noise}\rangle_{out}}{\langle i^2_{noise}\rangle_{in}} . \tag{2.1}$$

where $\langle i^2_{noise}\rangle_{in}$ and $\langle i^2_{noise}\rangle_{out}$ correspond to the amplifier input and output mean square noise currents in a unit bandwidth, respectively, and G is the amplifier gain. By definition, the ideal photodiode has a quantum efficiency of one. In addition, the only source of noise detected when measuring the input signal is assumed to be shot noise. Therefore, $\langle i^2_{noise}\rangle_{in}$ is given by,

$$\langle i^2_{noise}\rangle_{in} = 2\,e\,R^*\,P_{in} \tag{2.2}$$

where e is the electron charge, P_{in} is the amplifier optical input signal power, $R^* = e/h\nu$ is the responsivity of the IPD, h is Planck's constant, and ν is the optical frequency. $\langle i^2_{noise}\rangle_{out}$ is the output shot noise plus the additional noise from the EDFA in a unit bandwidth; this can be written as:

$$\langle i_{noise}^2 \rangle_{out} = 2\,e\,R^*\,P_{in}\,G + N_{EDFA,\,out} \tag{2.3}$$

where $N_{EDFA,\,out}$ is the EDFA mean square noise photocurrent in a unit bandwidth at the IPD, and can be written as,

$$N_{EDFA,\,out} = (R^*)^2 \langle (\Delta P_{optical})^2 \rangle \tag{2.4}$$

where $\langle (\Delta P_{optical})^2 \rangle$ is the mean square power fluctuation in a unit bandwidth of the EDFA output signal. By considering that real photodetectors (PD) have a quantum efficiency η, less than one, and the coupling efficiency between the EDFA output and PD is K_{in} (e.g. due to the connector loss), the EDFA mean square noise photocurrent in a unit bandwidth measured by a real photodiode, N_{EDFA}, can be written as,

$$N_{EDFA} = R^2 K_{in}^2 \langle (\Delta P_{optical})^2 \rangle \tag{2.5}$$

where $R = \eta e/h\nu$ is the responsivity of the real photodiode. From equations (2.1)-(2.5), and considering that $K_{in}R$ can be obtained by dividing the photodiode average current I by the EDFA output power $P_{in} \times G$, the EDFA noise figure equation can be written as:

$$NF = \frac{N_{EDFA}\ P_{in}}{2\,h\nu\,I^2} + \frac{1}{G} \tag{2.6}$$

Equation (2.6) is of particular significance as it shows that the EDFA noise figure can be

expressed in terms of three parameters P_{in}, G, and I, which can be measured easily and accurately. Therefore, the difficult problem of measuring NF has been reduced to an accurate determination of N_{EDFA}, which is considered next.

The factor N_{EDFA} was determined from measurements of the noise power at the input and output of EDFA using the experimental setup shown in Fig. 2.2. Using this setup, the noise power is measured using an HP 437B broadband radio-frequency average power meter (RFPM) over the 50-450 MHz passband of an electrical bandpass filter (EBPF). A distributed feedback laser (DFB) operating at the wavelength 1547.4nm is used as the EDFA input signal source, and optical attenuator A1 is used to vary the signal level at the EDFA input. Optical attenuator A2 is used to adjust the optical power level at the receiver input (P_{RX}). The optical bandpass filter (OBPF) has a passband of 2nm and is used to reduce the amplified spontaneous emission (ASE) power at the EDFA output, minimizing the effect of ASE-ASE beat noise. The receiver is an Ortel 2620A-E01 and consists of a photodiode (PD), and a transimpedance amplifier (TA); L_d is the total coupling loss from receiver input to PD. RFA is a wideband RF amplifier having a gain of 30dB and is used to minimize the effect of thermal noise in the RF power meter on the total measured noise power, enhancing the measurement dynamic range. IM is a 75Ω to 50Ω converter which matches the 75Ω output impedance of the receiver to the 50Ω input impedance of the RF amplifier. To minimize the influence of interferometric noise in the NF measurements, the EDFA in the setup has an input and output isolator to prevent multiple amplification of back scattered or reflected light, caused mainly by fiber Rayleigh scattering in the gain medium; also all the components in the setup have angled connectors with a return loss of more than 60 dB

and attenuators have reflectivities less than −55 dB. Furthermore, the DFB laser has a linewidth of approximately 1.5MHz which ensures that the interferometric noise has dropped significantly for frequencies above approximately 50MHz (see Section 1.4.2 for details or Ref. [35]). The DFB laser has a relative intensity noise (RIN) of -170±2 dB/Hz in the 50-450 MHz frequency range and such a small laser RIN makes the beat noise due to the interaction of the laser RIN with the ASE negligible [31].

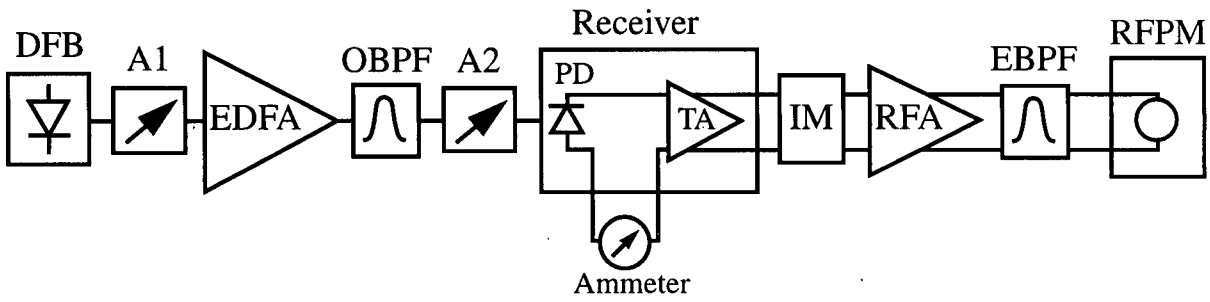

Figure 2.2: Experimental setup for broadband EDFA noise figure measurements; the components are described in the text.

The noise power measured by the RFPM, P_N, is obtained by integrating the noise over the entire signal bandwidth. By considering that the interferometric noise is significantly suppressed in the 50-450 MHz frequency range, it can be assumed that the noise current is constant over the measurement bandwidth (this assumption will be also justified experimentally in Section 2.5), and hence P_N can be written as:

$$P_N = \frac{N_{total} Z^2 B_n}{Z_{in}} + P_{th} \,, \tag{2.7}$$

where N_{total} is the total mean square noise photocurrent per unit bandwidth at the output of the photodiode receiver, Z is the transimpedance of the network which connects the photodiode to the power meter; B_n is the effective bandwidth of this network, which would normally be determined by the electrical bandpass filter shown in Fig. 2.2. Z_{in} is the input impedance of the power meter, and P_{th} is the noise power measured due to thermal noise generated in the power meter and the network connecting it to the photodiode. The total noise N_{total} is given by

$$N_{total} = N_{EDFA} + N_{RIN} + N_{shot} . \tag{2.8}$$

In this equation N_{RIN} describes source RIN noise per unit bandwidth and is given by

$$N_{RIN} = (P_{RX} L_d R)^2 \, RIN . \tag{2.9}$$

The shot noise per unit bandwidth N_{shot} is given by

$$N_{shot} = 2 \, e \, P_{RX} \, L_d \, R . \tag{2.10}$$

To obtain N_{EDFA}, the contributions of the RIN, shot, and thermal noise have to be excluded from the measured noise power P_N. However, the noise power due to these three extraneous noise terms is constant for a constant received power P_{RX}. Therefore N_{EDFA} can be determined from the measurement of noise power with and without the EDFA, maintaining identical

received optical power using attenuator A2. Thus

$$N_{EDFA} = \frac{(P_{N2} - P_{N1})\, Z_{in}}{Z^2\, B_n} \tag{2.11}$$

where P_{N2} and P_{N1} are the noise powers measured with and without the EDFA present, respectively. Finally, from equations (2.6) and (2.11) the following expression for the noise figure is obtained

$$NF = \frac{(P_{N2} - P_{N1})\, P_{in}\, Z_{in}}{2\, h\, \nu\, I^2\, Z^2\, B_n} + \frac{1}{G} \tag{2.12}$$

In the final noise figure equation, equation (2.12), all quantities, except the factor $(Z^2 B_n)/Z_{in}$, can be obtained simply and accurately by direct measurement. Direct measurement of the factor $(Z^2 B_n)/Z_{in}$ is not an easy task, as it requires access to internal circuitries of the receiver and RF power meter. Alternately, determination of the product $(Z^2 B_n)/Z_{in}$ can be accomplished accurately using the following calibration technique. This calibration technique relies upon the fact that, with the EDFA removed from the setup, the measured noise power P_N is proportional to the sum of source RIN, photodiode shot, and thermal noise terms; from equations (2.7), (2.9)-(2.10) and considering that $L_d R = I/P_{RX}$ this proportionality can be written as:

$$P_N = \left(\frac{RIN\, Z^2\, B_n}{Z_{in}}\right) I^2 + \left(\frac{2\, e\, Z^2\, B_n}{Z_{in}}\right) I + P_{th} \tag{2.13}$$

The second coefficient of the above equation contains the product $(Z^2 B_n)/Z_{in}$; this product can be obtained from a least squares fit of a quadratic function to a series of measurements of P_N at varying received power levels. The results of such a series of measurements are shown in Fig. 2.3 by open circles, and the solid line shows the quadratic fit. Accounting for the absolute uncertainties in the measurements of P_N and I, which are ±0.052 dB and ±0.022 dB, respectively, the accuracy of the $(Z^2 B_n)/Z_{in}$ determination is estimated to be ±0.076 dB [36].

Equation (2.13) is similar to equation (1.18), except that it replaces the two parameters of optical power and photodiode responsivity contained in equation (1.18) by a single parameter of photodiode average current. This enhances the accuracy for the following reasons: first, it eliminates the requirement of knowing the coupling loss between receiver input and photodiode, which is difficult to measure; second, it eliminates photodiode responsivity from the relation; and third, it replaces the optical power with average current, which can be measured with much higher accuracy.

The broadband NF measurement technique described above is appropriate if the NF is constant over the passband of the electrical bandpass filter. However, in many practical situations where the signal laser has a broader linewidth and/or optical isolators are not employed at the input and output of EDFA, multiple pass interference caused by various effects, such as multiple Rayleigh back scattering and reflections from downstream and upstream components of the transmission line, creates interferometric noise [37] and, since this noise is frequency dependent, frequency-resolved measurements of noise figure is desirable [35]. The electrical measurement technique described above can be extended to this case by replacing the electrical bandpass filter

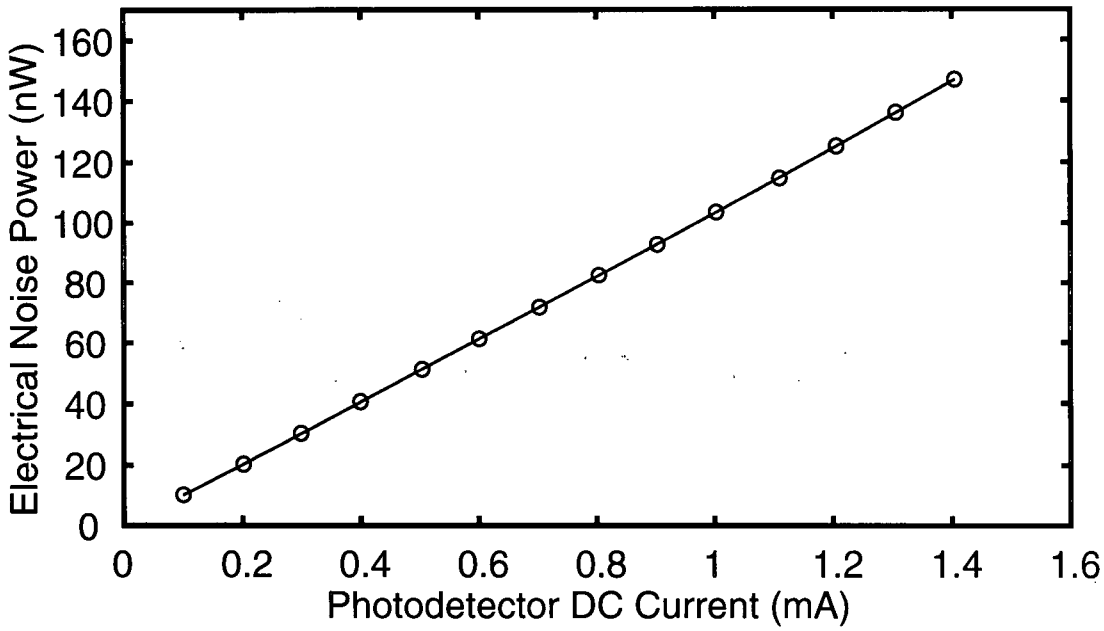

Figure 2.3: Calibration measurements: noise power P_N as a function of photodetector current I with the EDFA removed. The open circles show the measured data, and the solid line shows the least squares fit described in the text.

and the RF power meter with an electrical spectrum analyzer (ESA) in the measurement setup shown in Fig. 2.2. In this case, the spectrum analyzer measures the average noise power over a selected frequency span and within a selected resolution bandwidth and hence frequency-resolved measurements of NF can be achieved. Since the product $(Z^2 B_n)/Z_{in}$ could be frequency dependent, in frequency-resolved measurements of NF the calibration technique described for the broadband measurements should be performed for each baseband frequency.

2.4 Optical Noise Figure Measurements

To be able to compare the results of the electrical NF measurement technique with the optical NF, measurements of the optical NF were also performed. The measurement method used is based on the conventional polarization nulling technique, which is described in Section 1.5.1. In addition, a calibration technique was developed to enhance measurement accuracy. As described in Section 1.5.1, in the optical NF measurement technique, the ASE optical power P_{ASE} is measured at the signal wavelength using an optical spectrum analyzer (OSA), and then the optical NF is calculated from equation (1.2).

The experimental setup for the measurement of P_{ASE} is shown in Fig. 2.4. The DFB laser is the same laser used in the electrical measurements. The optical bandpass filter (OBPF) has a passband of 2nm and is used for calibration which will be discussed later. Attenuator A1 is used to adjust the EDFA input power. The EDFA output is passed through a polarization controller and a linear polarizer (MPB Technologies model B-001) with an extinction ratio greater than 40dB. The spectrum at the output of the polarizer is measured using an ANDO 6315B optical

spectrum analyzer. Using the polarization controller, the polarization state of the amplified signal is set orthogonal to the polarizer, and thereby the signal is suppressed by approximately 40dB, allowing measurements of the P_{ASE}. However, in highly saturated EDFAs where the ratio between the output signal power and P_{ASE} increases rapidly for higher input powers, this is not sufficient to eliminate the signal completely. As an example, the measured spectrum at the output of the polarizer for an EDFA input signal power of 0 dBm is shown in Fig. 2.5 by the lower curve; residual signal is evident at 1547.4nm. Due to the existence of this signal residue, a linear fit to values measured ±0.5 nm away from the signal wavelength is also used to estimate the ASE level at the signal wavelength [8]. However, due to the optical loss of the polarizer and the polarization controller, the measured ASE level is lower than the actual P_{ASE}. Since this loss factor varies at different settings of the polarization controller, its direct measurement is difficult. The appropriate method to determine this loss factor has not been discussed by previous authors; here, this loss is determined by performing the following simple calibration. First, the polarization controller and the polarizer are removed from the setup, and the EDFA output spectrum is measured directly; for the input signal power of 0 dBm this spectrum is shown as the upper curve in Fig. 2.5. At a wavelength separated from the signal wavelength by approximately 5 nm, the input signal is almost completely eliminated by the optical bandpass filter and the output spectrum at this wavelength represents the actual ASE level. Therefore at this wavelength, the difference between the two measured spectra shown in Fig. 2.5 is equal to the insertion loss. Finally, P_{ASE} is obtained by adding this insertion loss to the measured ASE level. Accounting for the accuracies of the OSA level measurements (±0.3 dB), linearity (±0.05 dB), polarization

dependency (±0.05 dB), and resolution bandwidth (±0.1 dB), the absolute uncertainty in the optical NF measurements is estimated to be ±0.5 dB.

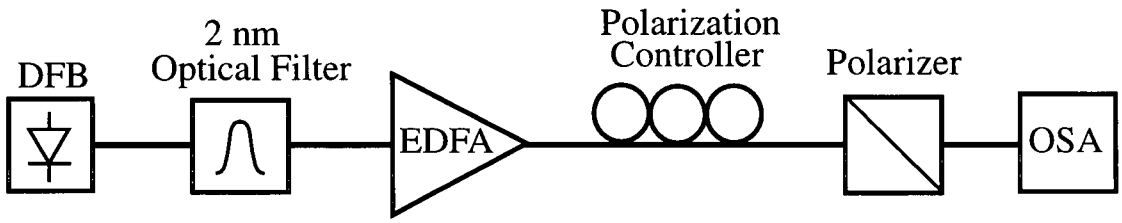

Figure 2.4: Experimental setup for optical NF measurements.

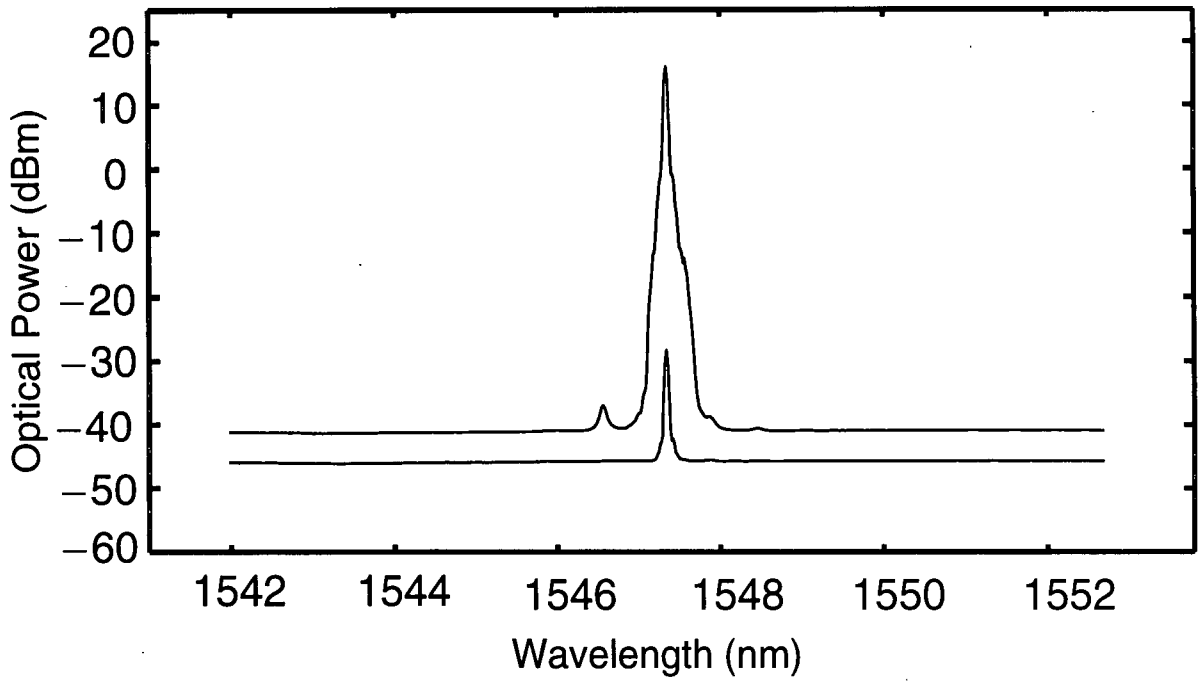

Figure 2.5:Experimental results of polarization nulling technique. The upper curve shows the spectrum at the EDFA output; the lower curve is the spectrum at the polarizer output, showing residual signal at 1547.4nm due to finite extinction ratio of the polarizer. The resolution of the optical spectrum analyzer is 0.1nm.

2.5 NF Measurement Results and Discussions

In this section results of optical and electrical NF measurements for two copropagating 980nm pumped EDFAs are presented and discussed. Both amplifiers use Er/Al/Ge/P doped fiber. EDFA1 has an input pump power of 20 dBm, and is built from 12 meters of doped fiber with an erbium concentration of 960 ppm-wt, core radius of $1.9\mu m$ and numerical aperture (NA) of 0.2. EDFA2 has an input pump power of 19 dBm and is built from 5 meters of the doped fiber having an erbium concentration of 2000 ppm-wt, core radius of $1.6\mu m$ and an NA of 0.24. Fig. 2.6(a) and 2.6(b) show results of NF and optical gain measurements for EDFA1 and EDFA2 respectively, as a function of the amplifier input signal power. Results of optical and broadband electrical NF measurements are shown as asterisks and open circles, respectively. The results of optical gain measurements are shown as squares. For broadband electrical measurements the uncertainty in determination of NF is estimated to be within ± 0.3 dB. This estimate is based on the uncertainties in the measurements of different parameters in equation (2.12). These uncertainties are ± 0.052 dB for electrical noise power measurements, ± 0.13 dB for optical power measurements, ± 0.022 dB for DC current measurements, and ± 0.076 dB for determination of the calibration parameter $(Z^2 B_n)/Z_{in}$.

For both amplifiers, the electrical and optical NF shown in Fig. 2.6 increase in saturation and there is an excellent agreement between the two measurements in this regime. Similar behavior has also been observed for several other EDFAs tested. This result is in contradiction to the results of Ref. [13]-[14] and throws into question the relevance of nonlinear photon statistics to saturated EDFAs. The agreement between the electrical and optical measurements worsens for

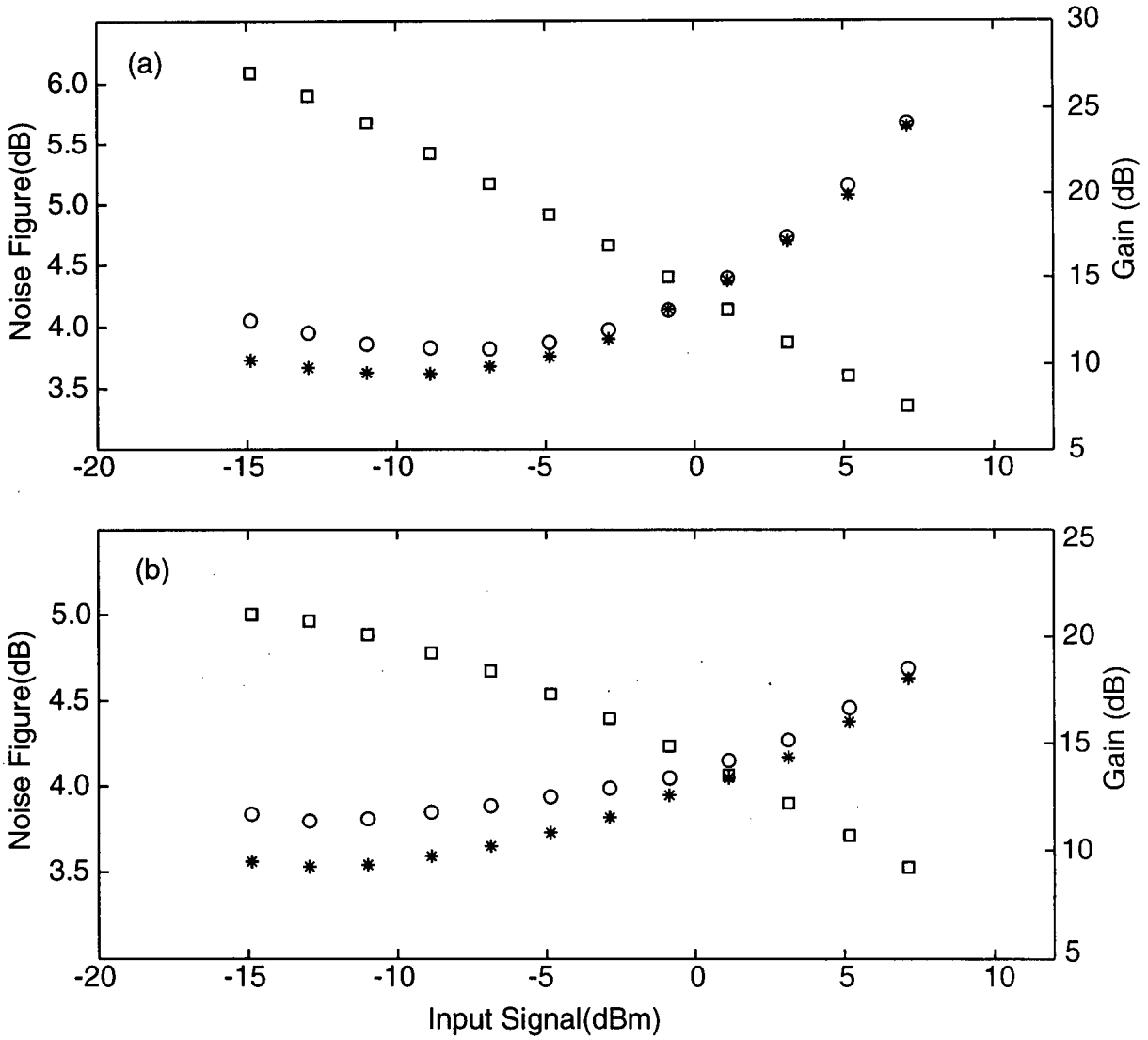

Figure 2.6: Measured gains and noise figures as a function of input signal power: (a) and (b) show results for EDFA1 and EDFA2, respectively. The open circles and asterisks show results of broadband electrical and optical NF measurements, respectively. The squares show results of optical gain measurements.

the lower input signal powers, where the electrical NF becomes larger than the optical NF. By considering that optical NF represents only signal-ASE beat noise, while electrical NF includes two additional terms of ASE-ASE beat noise and interferometric noise, one might expect that the discrepancy between the two measurements might be due to these two additional terms. To investigate the influence of ASE-ASE beat noise on the NF of EDFA1 and EDFA2, the following expression was used [31]

$$NF_t = \frac{P_{ASE}}{h\nu\,\Delta\nu\,G} + \frac{(P_{ase})^2}{2\,h\nu\,B\,P_{in}\,G^2} + \frac{1}{G}. \tag{2.14}$$

where NF_t represents the optical noise figure due to signal-ASE beat noise and ASE-ASE beat noise (the second term in the above expression). B is the passband of the optical filter, which is 2nm for this case and P_{ase} is the amplifier ASE power within the passband of the optical filter. P_{ase} was calculated from equation (1.2) by replacing $\Delta\nu$ with B and using the measured optical NF results. Calculations of NF_t for both EDFA1 and EDFA2 have shown that the maximum contribution of ASE-ASE term is only 0.005 dB, which occurs at lowest input signal power of -15 dBm. Therefore, ASE-ASE beat noise should have negligible effect on the NF results presented in Fig. 2.6. To investigate the influence of the interferometric noise on the NF of EDFA1 and EDFA2, frequency-resolved noise figure measurements were also performed. These measurements were obtained with a Rohde&Schwarz FSEA 20 spectrum analyzer. In these measurements, the resolution bandwidth of the spectrum analyzer was 10 MHz, and the video filter bandwidth was 5Hz. Fig. 2.7 shows results of the frequency-resolved noise figure measurements

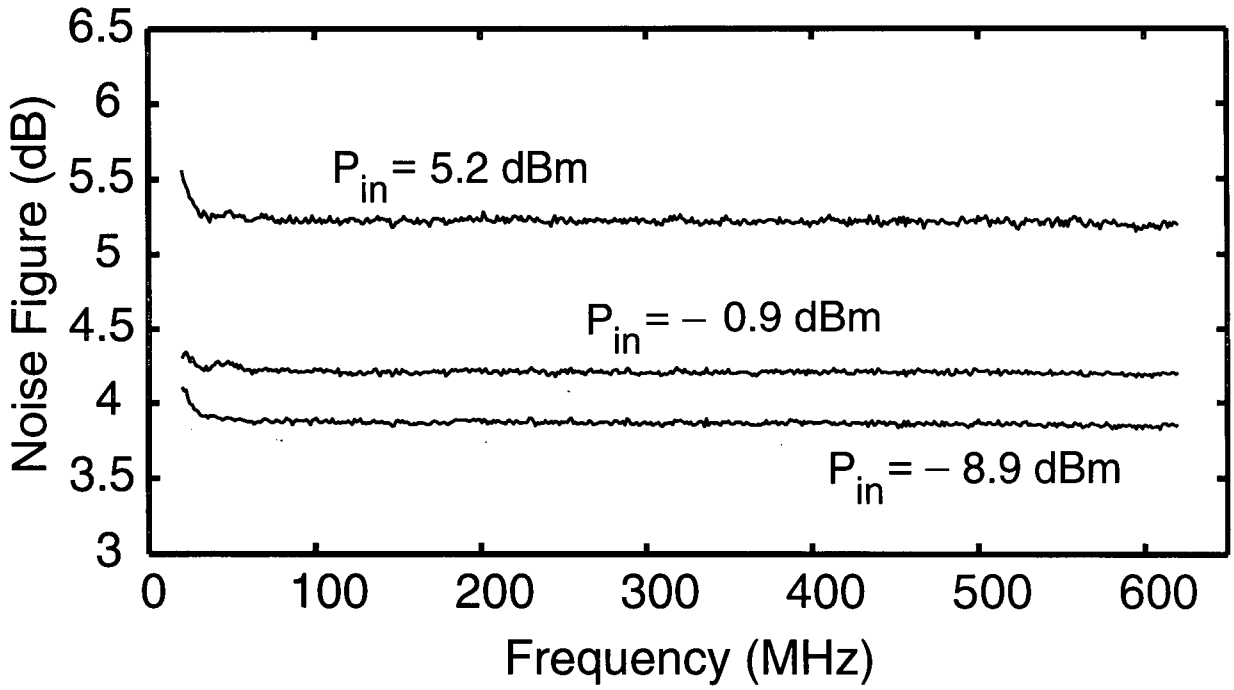

Figure 2.7: Frequency-resolved noise figure for EDFA1 at input powers of -8.9, -0.9, and 5.2 dBm, respectively, as labeled.

for EDFA1 at three input signal powers. For frequencies below 30MHz the NF increases considerably with frequency, but for frequencies above 30MHz the noise figure is almost constant having an inconsiderable negative slope. This increase of the NF at low frequencies is due to the presence of the interferometric noise; however, as it was explained earlier, since the laser linewidth is 1.5MHz, the effect of this noise term becomes almost negligible for higher frequencies. The fact that the NF is almost flat in the frequency span of the electrical bandpass filter (50-450MHz) on one had confirms the validity of the broadband NF measurements and on the other hand suggests that the contribution of the interferometric noise to the total NF of EDFA1 and EDFA2 should be negligible. As a result, the discrepancy between the electrical and optical NF measurements in Fig. 2.6 can be neither due to ASE-ASE beat noise nor interferometric noise. Therefore this discrepancy is expected to be due to some unknown measurement artifacts; one possibility being the OSA and RFPM nonlinearity. However, considering the measurement uncertainties discussed earlier, it is obvious that there is an excellent agreement between the optical and electrical NF results presented in Fig. 2.6.

In Table 2.1, the average value of the frequency-resolved measurements of NF in the frequency range of 50-450 MHz are compared with the ones obtained from the broadband measurements. This comparison shows an excellent agreement between the two approaches. Neglecting the nonlinearity of the ESA level measurements, the accuracy of the frequency-resolved NF measurements is also within ± 0.3 dB.

TABLE 2.1: Comparison between the mean values of the NF measured using an electrical spectrum analyzer with those measured with a broadband RF power meter.

EDFA Input Power (dBm)	Mean of Frequency-Resolved NF (dB)	Broadband NF (dB)
−8.9	3.92	3.83
−0.9	4.21	4.13
5.2	5.23	5.16

2.6 Summary and Conclusions

A simple electrical NF measurement method was described, which has an absolute accuracy of ±0.3 dB for the measurements presented; this accuracy is significantly better than conventional RIN subtraction technique results reported to date. The accuracy of the conventional polarization nulling technique for optical NF measurements was enhanced by introducing a simple calibration method. For the case of several EDFAs tested, an excellent agreement was found between the electrical and optical NF measurements in saturation. These results are in contrast to previous reports where significant differences between the two measurements have been observed, and throws into question the applicability of nonlinear photon statistics in erbium-doped fiber amplifiers.

Chapter 3

Design and Modeling of Saturated Erbium-Doped Fiber Amplifiers

3.1 Introduction

As described in Chapter 1 erbium-doped fiber amplifiers operating in signal-saturated regime have become the key components of the rapidly growing wavelength division multiplexed (WDM) and cable television (CATV) optical communication systems. Therefore, design for high efficiency, and simple and accurate theoretical modeling of gain and noise figure in saturated EDFAs is of prime importance. This chapter describes new approaches for efficient design of saturated EDFAs and for the modeling of gain and noise figure in EDFAs.

The organization of this chapter is as follows. In Section 3.2, motivation of the work presented in this chapter is described. In Section 3.3, using a general model, it is shown that in signal-saturated EDFAs the effect of ASE on the gain and NF performance of amplifiers is negligible and that highest-efficiency operation of saturated EDFAs is achieved with erbium distributed throughout the entire fiber core. In Section 3.4, gain and noise figure predictions of Saleh's model, for a non-confined 980nm pumped EDFA, are compared with predictions of the general model, and it is shown that Saleh's model cannot accurately predict the performance of non-confined EDFAs. In Section 3.5, a simple model for co-propagating 980-nm-pumped EDFAs is derived. This model incorporates commonly neglected effects of pump excited state

absorption and fiber background losses at the signal and pump wavelengths. It is shown that the saturation parameters normally contained in conventional models can be eliminated without compromising the accuracy, with the resulting model requiring only small signal gain and loss coefficients as parameters. Gain and noise figure predictions of the resulting model are shown to be in excellent agreement with the predictions of the general model. In Section 3.6 a new method for determining the pump excited state absorption coefficient is presented and experimental methods used for measuring the parameters contained in the proposed model are described. Excellent agreement between predictions of the proposed model with the measured gain and noise figure of a 980-nm pumped EDFA is demonstrated. In Section 3.7 it is shown that the proposed model can be extended to model a wide variety of practical EDFAs, including commonly used pump wavelengths and configurations. Finally, conclusions are presented in Section 3.8.

3.2 Motivation

It is generally believed that efficient EDFAs should be designed with confined erbium doped fibers (EDFs), that is, fibers where the erbium doping is confined near the center of the EDF core [2]-[4], [17], [38]-[41]. The logic behind this argument is that the pump mode envelope is maximum at the fiber center and therefore a higher population inversion can be achieved by concentrating the erbium ions near the core center. This is claimed to result in a larger ratio of signal to amplified spontaneous emission (ASE), which will result in higher amplifier gain and lower noise figure. This claim is correct for small-signal amplifiers. However, here it is shown that in

signal-saturated EDFAs, the effect of ASE on the population inversion is negligible, and that in the presence of fiber background loss, non-confined EDFAs can have improved efficiency, gain and noise figure in saturated operation.

Accurate modeling of gain and noise figure in non-confined EDFAs has not been considered in previous work. The comprehensive model and the effective ASE model (described in Section 1.6) which include the radial optical fields and erbium distribution are most suitable for accurate modeling of such amplifiers. However, these models are not very practical as they include many parameters, some of which are difficult to measure accurately. On the other hand, the applicability of the widely used Saleh's model (described in Section 1.6) to non-confined EDFAs was never discussed in previous work. Nevertheless, it is not expected that this model provide accurate prediction of the performance of non-confined EDFAs. This is because the fundamental assumption in this model is that the erbium is so confined near the center of the fiber, such that the radial mode envelope distributions at the signal and pump wavelengths are identical in the doping region. When the EDF is non-confined, and especially when it is pumped at 980nm, the discrepancy between the pump and signal mode envelopes becomes large, and causes errors in predictions of the model [42]. In addition, the particular structure of this model does not allow inclusion of pump excited state absorption and fiber background loss at the signal and pump wavelengths. The parameters required in Saleh's model are the small signal loss coefficients and intrinsic saturation powers at the signal and pump wavelengths. While the loss coefficients can be precisely obtained using only relative measurements, the saturation powers, which are generally determined from monochromatic loss measurements using a transcendental equation (equa-

tion (1.13) derived in Ref. [19], are less accurately known. There are two reasons for this inaccuracy: first, measurement of absolute optical powers is required, second the transcendental equation used in obtaining the saturation powers from the monochromatic loss measurements ignores the effect of ASE which can be important. Therefore, the accuracy of the Saleh's model is also limited by the accuracy of the intrinsic saturation powers. In Section 3.5 a simplified one-dimensional steady-state model for gain and noise in saturated EDFAs is derived which is accurate for both confined and non-confined EDFAs [43].

3.3 Effect of Erbium Confinement on the Performance of Saturated EDFAs

In this Section, it is shown that in contrast to generally-accepted EDFA design principles, highest-efficiency operation of EDFAs is achieved by not confining the erbium but distributing it throughout the fiber core. First, using the effective ASE model, which will be referred to as the general model, the impact of the ASE on the gain and noise figure performance of a saturated 1550nm amplifier incorporating non-confined EDF is analyzed. This amplifier, which will be referred to as EDFA1, has the following parameters: fiber core radius $1.8\mu m$, numerical aperture 0.2, step-like erbium doping with a concentration of 5×10^{24} m^{-3}. The erbium confinement factor is 1, i.e. erbium is distributed across the entire fiber core. The spontaneous emission lifetime is taken to be 10ms, the effective ASE bandwidth as 2.6THz [17], [44]. The signal absorption and emission cross sections are taken as 2×10^{-25} and 3×10^{-25} m^2, respectively, and pump absorption cross section is 2×10^{-25} m^2. The EDF length is 7m and the input pump power is 125 mW. For the present comparison, background losses and ESA are ignored.

Fig. 3.1 shows the gain and NF of EDFA1 versus input signal power for two different effective ASE bandwidths: the asterisks show results for the nominal value, while the circles show the results where $\Delta\nu_{eff}$ is set to a very small value, effectively eliminating the ASE influence on the population inversion. The near perfect agreement of the two results in Fig. 3.1 shows that even in the present case where the erbium doping extends throughout the core, no error is incurred by ignoring the ASE effect on population inversion. To confirm that this result is not highly sensitive to the exact value of the effective ASE bandwidth, similar calculations were performed with $\Delta\nu_{eff}$ artificially increased by a factor of three; results are shown in Fig. 3.2 and are nearly indistinguishable from those in Fig. 3.1.

Second, the general model is used to compare the saturated performance of two amplifiers with differing confinement, which will be referred to as EDFA2 and EDFA3. In making a realistic comparison, it is essential to include the effect of fiber background loss coefficients at the signal and pump wavelengths. For the present case these are taken as 0.03 and 0.08 dB/m, respectively, which are typical values for aluminum co-doped EDFs [45]-[46]. EDFA2 has a length of 10m, and other parameters are the same as in EDFA1 described above; EDFA3 is identical, except for a confinement factor of 0.5 and a length of 25m. The comparison is performed at an input signal power of 0dBm. The two EDF lengths have been chosen such that the residual pump powers are approximately 10dBm; this value is somewhat arbitrary but is typical for the pump and signal powers chosen here; however, the exact value chosen does not affect the conclusion drawn below. Table 3.1 shows the result of the comparison, and EDFA2, which is non-confined, has approximately 1dB higher gain compared to EDFA3, which is confined. The supe-

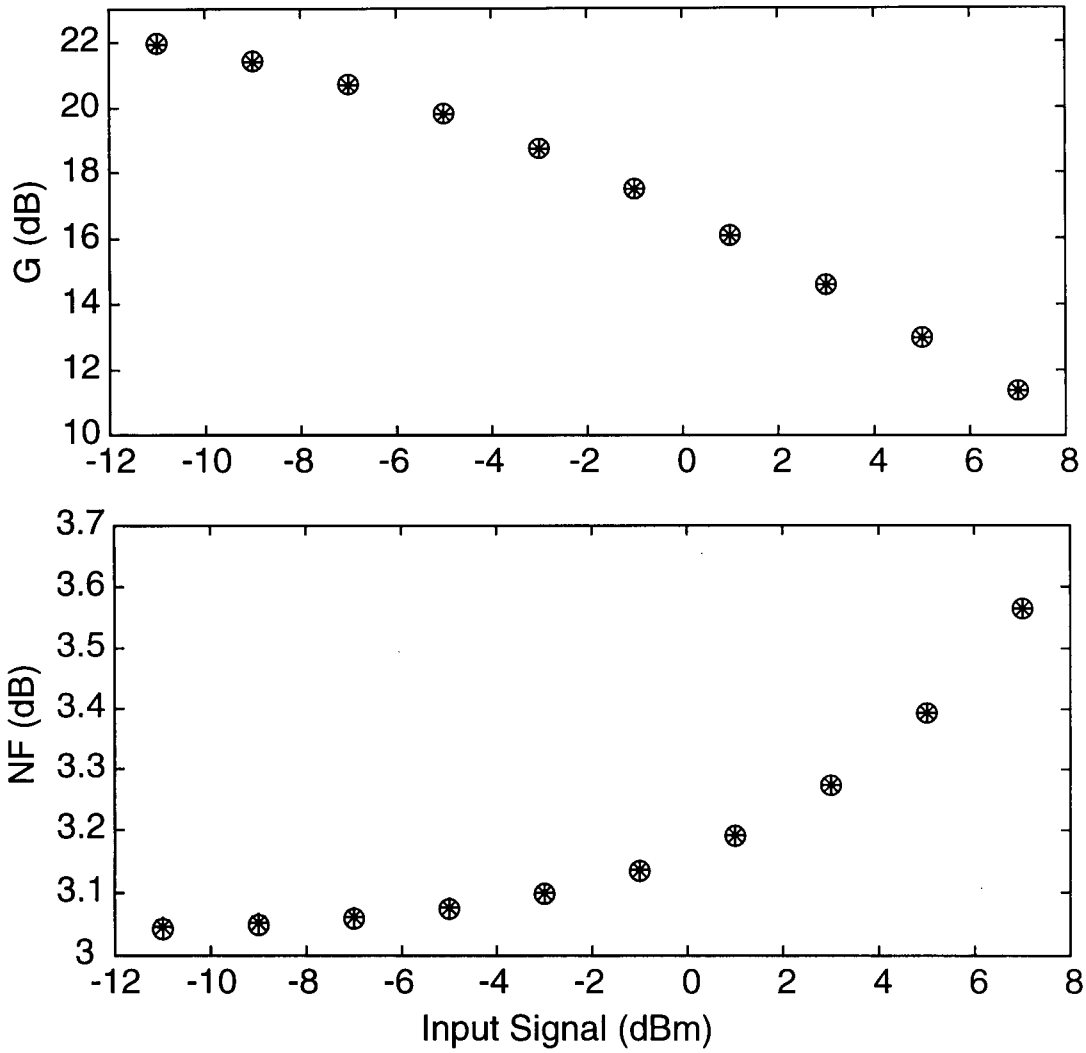

Fig. 3.1: Theoretical results, using the general model, for gain and noise figure versus input signal power for EDFA1 which has an erbium confinement factor of 1. Open circles and asterisks show the results for cases that ASE effects on population inversion are neglected and included, respectively.

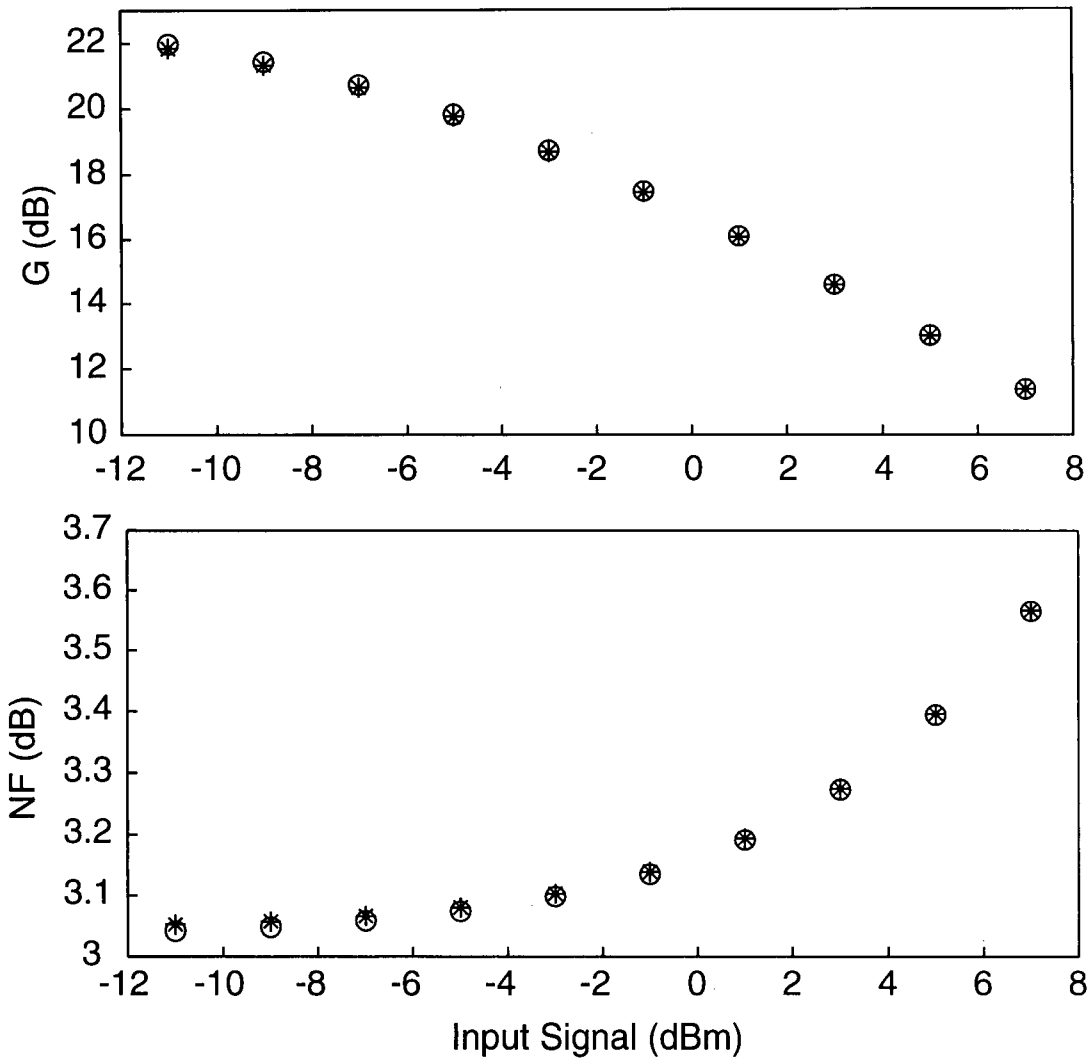

Fig. 3.2: Theoretical results, using the general model, for gain and noise figure versus input signal power for EDFA1 which has an erbium confinement factor of 1. Open circles show the result for the case that ASE effect is neglected and asterisks show the results for the case that ASE is included and its effective bandwidths is artificially increased by a factor of 3.

rior performance of the non-confined amplifier is due the fact that its optimized length is 2.5 times shorter compared to the confined case, and therefore fiber background losses at the signal and pump wavelengths have less deleterious effects on its performance. The shorter optimized length of the unconfined EDFA is due to its higher gain per unit length which occurs because of its larger erbium content per core area.

Table 3.1: Theoretical comparison of gain and NF of two EDFAs; EDFA2 and EDFA3 which have erbium confinement factor of 1 and 0.5, respectively. Other parameters are given in the text.

Amplifier	Length(m)	Gain(dB)	NF(dB)	Residual Pump(dBm)
EDFA2	10	17.72	3.28	9.76
EDFA3	25	16.73	3.31	9.80

3.4 Assessment of Saleh's Model Accuracy for Non-Confined EDFAs

In the previous section it was shown that non-confined EDFAs operating in signal saturated regime have a superior performance compared to confined ones. In this section, the accuracy of the widely used Saleh's model for predicting gain and noise figure of non-confined EDFAs is examined.

To assess the accuracy of Saleh's model for non-confined EDFAs, gain and noise figure pre-

dictions of this model for the case of EDFA1 are compared versus predictions of the general model. Since Saleh's model does not include the effect of fiber background losses and ESA, they are ignored in this comparison. The required parameters for Saleh's model are α_s, α_p, P_s^{sat}, and P_p^{sat} which are small signal loss coefficients and intrinsic saturation powers at the signal and pump wavelengths, respectively. These parameters are generally obtained from monochromatic loss measurements, at the signal and pump wavelengths, over a length of EDF, and fitting of the transcendental equation (1.13) to the measured results [19]-[20]. Here, these parameters are calculated based on the same approach described above, but using the general model to simulate the loss measurements. A 3 m length of EDF was considered, and the monochromatic loss at the signal and pump wavelengths were calculated for input powers ranging from -40 to 0dBm. Subsequently, the parameters α_s, α_p, P_s^{sat}, and P_p^{sat} were obtained from the least-squares fit of equation (1.13) to the monochromatic loss calculation and were calculated as 2.25dB/m, 3.77dB/m, 0.489 mW and 1.036mW, respectively. These parameters were then used in equations (1.13)-(1.16) of Saleh's model to calculate gain and noise figure of EDFA1. In Fig 3.3 results of monochromatic loss calculation and the least-squares fits used to obtain the small signal loss coefficients and saturation parameters are illustrated. The open circles show the monochromatic loss and the solid curves are the least-squares fits; the upper and lowers panels show results for the signal and pump wavelengths, respectively.

Fig. 3.4 shows theoretical prediction of the two models for the gain and noise figure of EDFA1; asterisks show predictions of the general model and squares show predictions of Saleh's model. From the results shown in Fig. 3.4 it is evident that Saleh's model cannot accu-

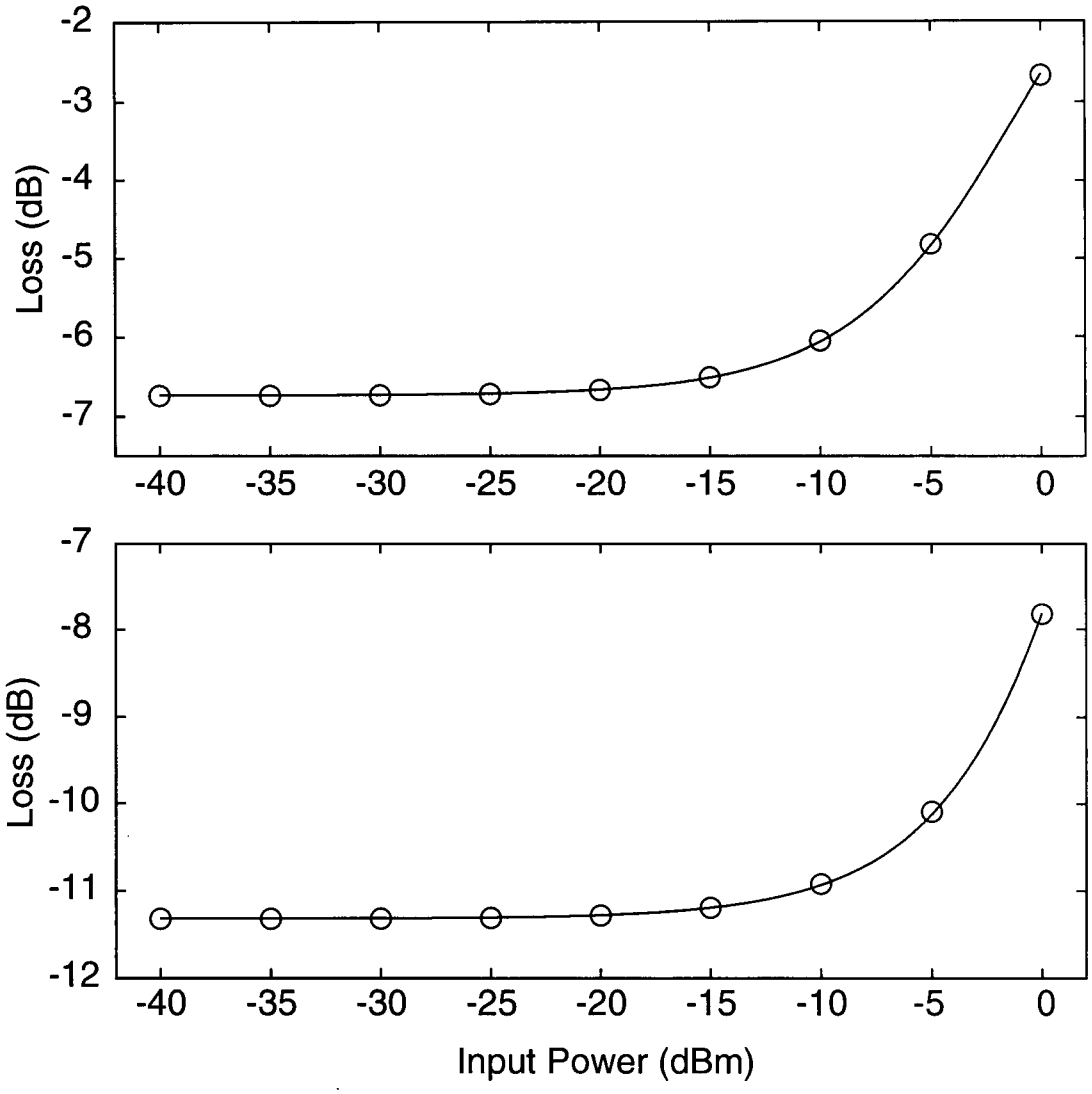

Fig. 3.3: Theoretical results of monochromatic loss (open circles) versus input power for 3m of the EDF used in EDFA1, and the least square fits (solid curves) used to obtain small signal loss coefficients and saturation parameters. The upper panel shows the results for the signal wavelength at 1550nm and the lower panel shows the results for the pump wavelength at 980nm.

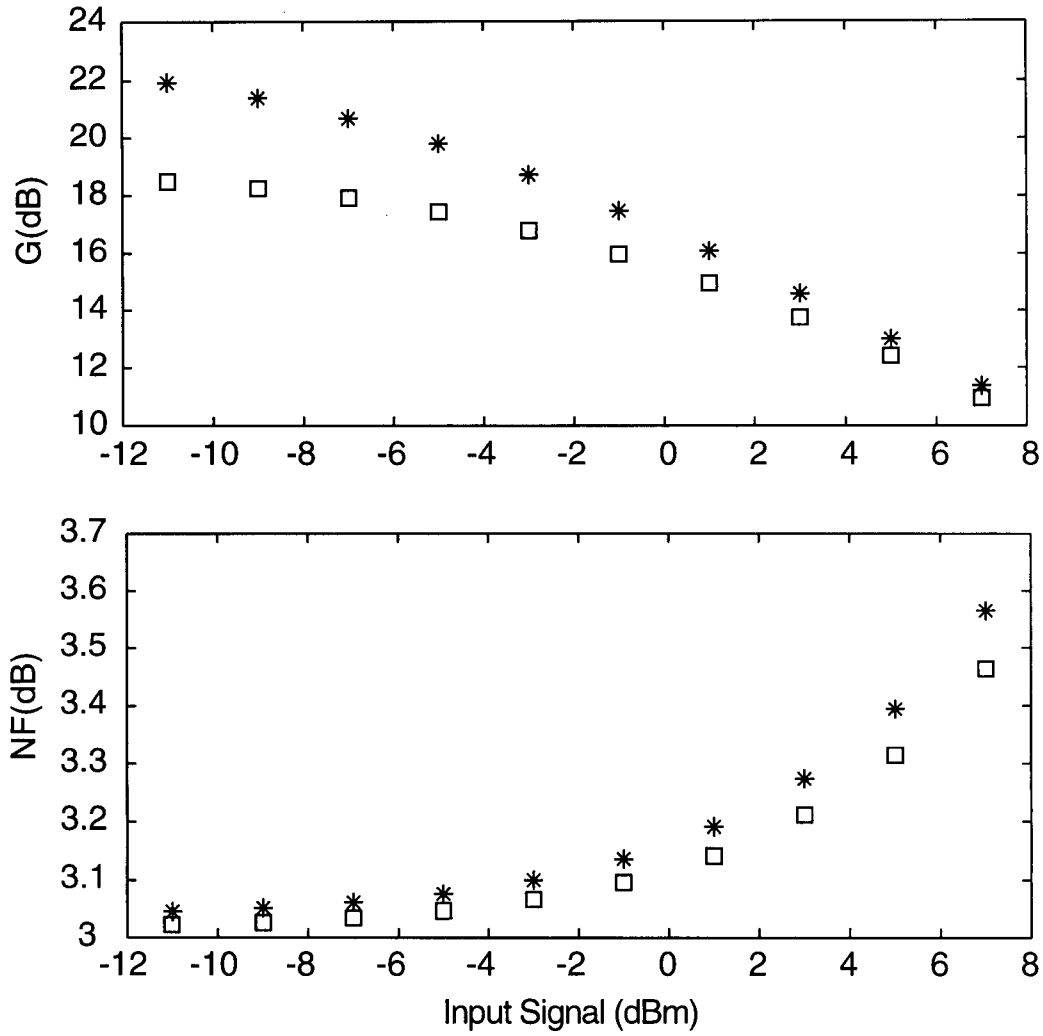

Fig. 3.4: Theoretical gain and NF comparison of the general model (asterisks) with the Saleh's model (squares) for the case of EDFA1 with an erbium confinement of 1.

rately predict the gain and NF performance of non-confined EDFAs. This is due to the fact that in Saleh's model it is assumed that the erbium is well confined inside the fiber core such that the overlap integrals between the erbium and the optical modes are equal at the signal and pump wavelengths. When EDF is non-confined and especially when it is pumped at 980nm, the discrepancy between the overlap integrals at the signal and pump wavelengths become large, causing errors in predictions of the model.

3.5 A Simple and Accurate Model for Saturated EDFAs

In this section, from the general model, a one-dimensional model is derived which can closely predict the gain and noise figure of confined and non-confined saturated EDFAs and as parameters contains only small signal gain and loss coefficients.

Starting from the general model, the first simplification is made by assuming that ASE has negligible effect on the population inversion, which is well justified for the case of saturated EDFAs as shown in Section 3.3. Considering the general, radially-dependant propagation equations (1.5) and (1.6), four propagation constants that correspond to various specialized situations can be identified. The first, for no pump and small signal, i.e. $n_2(r) \approx 0$, is

$$\alpha_s = \frac{2\,\sigma_{sa}\,\Gamma_s}{\omega_s^2} \tag{3.1}$$

where

$$\Gamma_s = \int_r \rho(r)\psi_s(r)rdr \tag{3.2}$$

is the overlap integral for the signal wavelength. The propagation constant α_s is the signal absorption coefficient in the absence of the fiber background loss. The second, for small signal and strong 980nm pumping, where complete population inversion is achieved, i.e. $n_2(r) \approx 1$, is

$$g_s = \frac{2\,\sigma_{se}\,\Gamma_s}{\omega_s^2} \tag{3.3}$$

where g_s is the small signal gain coefficient in the absence of fiber background loss. The third, for no signal and small pump power, i.e. $n_2(r) \approx 0$, is

$$\alpha_p = \frac{2\,\sigma_{pa}\,\Gamma_p}{\omega_p^2} \tag{3.4}$$

where

$$\Gamma_p = \int_r \rho(r)\psi_p(r)rdr \tag{3.5}$$

is the pump overlap integral and α_p is the pump absorption coefficient in the absence of the fiber background loss, and finally,

$$\alpha_{ESA} = \frac{2\,\sigma_{ESA}\,\Gamma_p}{\omega_p^2} \tag{3.6}$$

is the excited state absorption coefficient, which obtains in the case of full inversion and negligible signal and ASE power. Note that all the absorption coefficients are positive quantities.

The above equations (3.1)-(3.6) can be used to eliminate microscopic cross sections in the propagation equations (1.5) and (1.6) yielding

$$\frac{dP_s}{dz} = \frac{P_s}{\Gamma_s}(\alpha_s + g_s)\int \rho(r)\; n_2(r)\; \psi_s(r)\, r\, dr \;-\; (\alpha_s + \alpha'_s)P_s \tag{3.7}$$

and

$$\frac{dP_p}{dz} = \frac{P_p}{\Gamma_p}(\alpha_p - \alpha_{ESA})\int \rho(r)\; n_2(r)\; \psi_p(r)\, r\, dr \;-(\alpha_p + \alpha'_p)\, P_p. \tag{3.8}$$

The next step is to eliminate the radially dependent functions in equations (3.7)-(3.8). This can be easily achieved if one assumes that $n_2(r)$ is constant all across the doped region. Obviously this is not generally the case; however a close examination of equation (1.8) shows that for the case of saturated EDFAs, where the signal and pump are relatively large, $n_2(r)$ remains almost constant across the entire core of the erbium-doped fiber. This is due to fact that $n_2(r)$ is determined by the ratios of two functions which are nearly similar. For a quantitative assessment of this claim, for the case of EDFA1, $n_2(r)$ was calculated versus EDF core radius at three loca-

tions along the length of the EDF. The results are shown in Fig. 3.5 depicting $n_2(r)$ versus EDF core radius at the input, middle and at the end of the EDF. Fig. 3.5 shows that $n_2(r)$ remains nearly constant across the entire fiber core. Taking advantage of this fact, an effective population density for the second level N_2 is defined which, with good approximation, can simultaneously satisfy the following relations:

$$N_2 = \frac{1}{\rho_t}\int_r \rho(r)\, n_2(r)\, r\, dr = \frac{1}{\Gamma_s}\int_r \rho(r)\, n_2(r)\, \psi_s(r)\, r\, dr = \frac{1}{\Gamma_p}\int_r \rho(r)\, n_2(r)\, \psi_p(r)\, r\, dr \tag{3.9}$$

where

$$\rho_t = \int_r \rho(r) r dr \tag{3.10}$$

From equations (3.7)-(3.9), the propagation equations for the signal and pump can be written as:

$$\frac{dP_s}{dz} = (\alpha_s + g_s)\, N_2\, P_s - (\alpha_s + \alpha_s')\, P_s \tag{3.11}$$

and

$$\frac{dP_p}{dz} = (\alpha_p + \alpha_p')(N_2 - 1)\, P_p - (\alpha_p' + \alpha_{ESA})\, N_2\, P_p \tag{3.12}$$

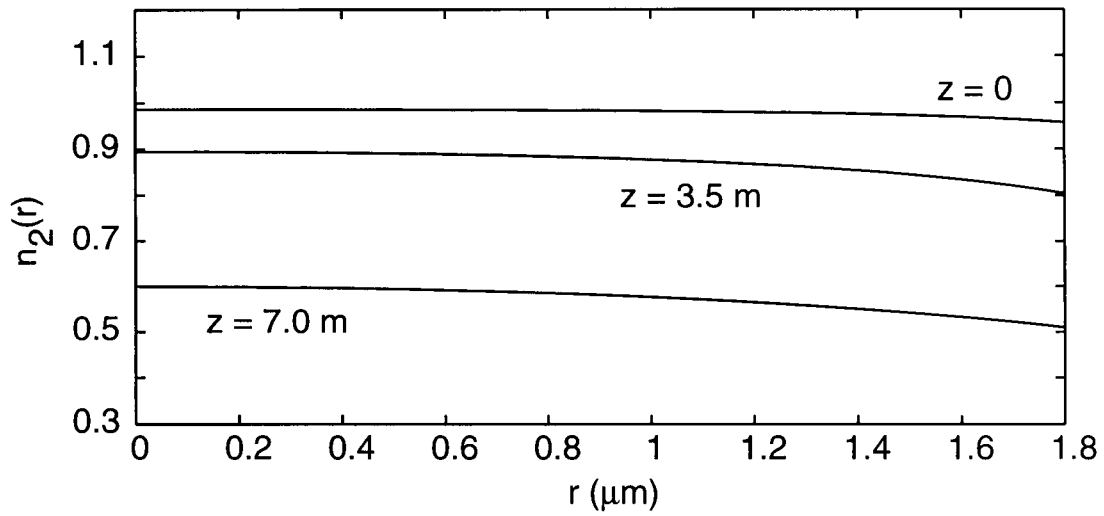

Fig. 3.5: Normalized population of the excited level $n_2(r)$ versus fiber radial coordinate r at three different locations (entrance, middle and exit) of EDFA1 as indicated in the figure.

The equation for N_2 can be obtained from equation (1.8) by using equations (3.1)-(3.6) to replace the cross sections, multiplying by $r\,\rho(r)$, integrating, and finally using equation (3.9) to yield

$$N_2(z) = \frac{\dfrac{P_p(z)}{\bar{P}_p^{sat}} + \dfrac{\alpha_s}{\alpha_s + g_s}\dfrac{P_s(z)}{\bar{P}_s^{sat}}}{1 + \dfrac{P_p(z)}{\bar{P}_p^{sat}} + \dfrac{P_s(z)}{\bar{P}_s^{sat}}} \tag{3.13}$$

where

$$\bar{P}_s^{sat} = \frac{2\pi h \nu_s \rho_t}{(\alpha_s + g_s)\,\tau} \tag{3.14}$$

and

$$\bar{P}_p^{sat} = \frac{2\pi h \nu_p \rho_t}{\alpha_p \tau} \tag{3.15}$$

are effective saturation powers at the signal and pump wavelengths, respectively. The resulting set of equations (3.11)-(3.13) is suitable for modeling saturated, 980nm-pumped, copropagating EDFAs including those with unconfined erbium doping [42].

The above model depends on the determination of saturation parameters which, as mentioned in Section 1.6, are less accurately known compared to loss and gain coefficients. Therefore, the accuracy of the model can be improved if saturation parameters can be eliminated from

the model. In addition, it is obvious that eliminating these parameters is desirable if accuracy can be maintained. In the following, it is shown that how this can be achieved. First consideration is that for typical EDFs, the saturation parameters at the signal and pump wavelengths, $\bar{P}_s^{sat}$ and $\bar{P}_p^{sat}$, are on the order of 0.5 and 1mW, respectively, and second is that in almost all practical saturated EDFAs, the input signal power and input pump power are so large that the sum of $P_p^{in}/\bar{P}_p^{sat}$ and $P_s^{in}/\bar{P}_s^{sat}$ which are the normalized number of pump and signal photons entering the amplifier, respectively, is much bigger than 1. Since in saturated EDFAs the ASE power is negligible, and the background loss and ESA coefficients are small, as the signal and pump propagate inside the amplifier only a small fraction of the total input photons will be lost. In other words, it is almost true that for each pump photon that disappears, one signal photon will be created. On the other hand, combination of (3.14) and (3.15) gives the following proportionality

$$\frac{P_p(z)}{\bar{P}_p^{sat}} + \frac{P_s(z)}{\bar{P}_s^{sat}} \propto \alpha_p N_p + (\alpha_s + g_s) N_s \tag{3.16}$$

where, N_p and N_s are the number of pump and signal photons, respectively. By considering that $\alpha_s + g_s > \alpha_p$, from (3.16) it is apparent that the factor $(P_p(z)/\bar{P}_p^{sat} + P_s(z)/\bar{P}_s^{sat})$ grows proportionally with conversion of pump photons to signal photons, and therefore it always remains bigger than $(P_p^{in}/\bar{P}_p^{sat} + P_s^{in}/\bar{P}_s^{sat})$ over the entire amplifier length. Consequently, 1 in the denominator of equation (3.13) can be ignored and using equations (3.14) and (3.15), N_2 can be written as:

$$N_2 = \frac{\dfrac{\alpha_p P_p(z)}{\nu_p} + \dfrac{\alpha_s P_s(z)}{\nu_s}}{\dfrac{\alpha_p P_p(z)}{\nu_p} + \dfrac{(\alpha_s + g_s) P_s(z)}{\nu_s}} \tag{3.17}$$

Hence, the saturation parameters can be eliminated from the model, not only making the EDF characterization easier but also making the model more accurate. This simplification is equivalent to letting the factor ρ_t/τ in equations (3.13)-(3.15) tend to zero, which is only possible if τ tends to infinity; this physically means that the spontaneous emission has negligible effect in determining the inversion level, which is the case for saturated EDFAs as shown in Section 3.2.

The proposed model is based on equations (3.11), (3.12), and (3.17): by solving these equations amplifier gain and population of the excited state are obtained. Then the noise figure can be calculated from equation (1.2) and using equation (1.15) to calculate the amplified spontaneous emission at the amplifier output:

$$NF = \frac{2\, g_s}{G} \int_0^L N_2 \, (P_s(L)/P_s(z)) \, dz + \frac{1}{G} \tag{3.18}$$

where $P_s(L)/P_s(z)$ corresponds to the gain the spontaneous emission, generated in an infinitesimal length of dz, experiences from position z to the amplifier output.

To compare predictions of the proposed model with the results of the general model, gain and NF of a copropagating 980nm-pumped amplifier, EDFA4, were calculated versus input sig-

nal power. This amplifier is assumed to have the same parameters as EDFA1 plus an α_s' of 0.03dB/m and α_p' of 0.08 dB/m. The general model was used to determine the small signal gain and loss coefficients required for the proposed model and the results were as follows: α_s=2.25 dB/m, g_s=3.37 dB/m, α_p=3.77 dB/m. Fig. 3.6 shows theoretical predictions of the two models for the gain and NF of EDFA4, respectively; asterisks show predictions of the general model and circles show predictions of the present model. Despite the fact that EDFA4 is non-confined, the agreement between the two models is excellent, showing the applicability of the proposed model to saturated EDFAs, even in the case of an erbium confinement factor as great as 1. To show the validity of the assumption made in simplifying the expression for N_2, in Fig. 3.7 the normalized pump and signal photon numbers, $P_p(z)/\bar{P}_p^{sat}$ and $P_s(z)/\bar{P}_s^{sat}$, are plotted versus EDF4's longitudinal coordinate z, at an input signal power of 0dBm; the solid line shows the normalized pump photon numbers and the dashed line shows the normalized signal photon numbers. The parameters $\bar{P}_s^{sat}$ and $\bar{P}_p^{sat}$ were calculated from equations (3.14) and (3.15) and were determined to be 0.50 and 1.19mW, respectively. As can be seen from Fig. 3.7, while $P_p(z)/\bar{P}_p^{sat}$ decreases, $P_s(z)/\bar{P}_s^{sat}$ increases, and the sum of the two always remain well above 1 justifying the assumption made in deriving equation (3.17).

3.6 EDF Characterization Methods and Measurements

In this section methods of characterization for the EDF parameters contained in the proposed model of Section 3.5 are described for the case of 980nm pumping. In the experiments conducted, an Er/Al/Ge/P doped fiber, which will be referred to as EDF5, was used in amplifier

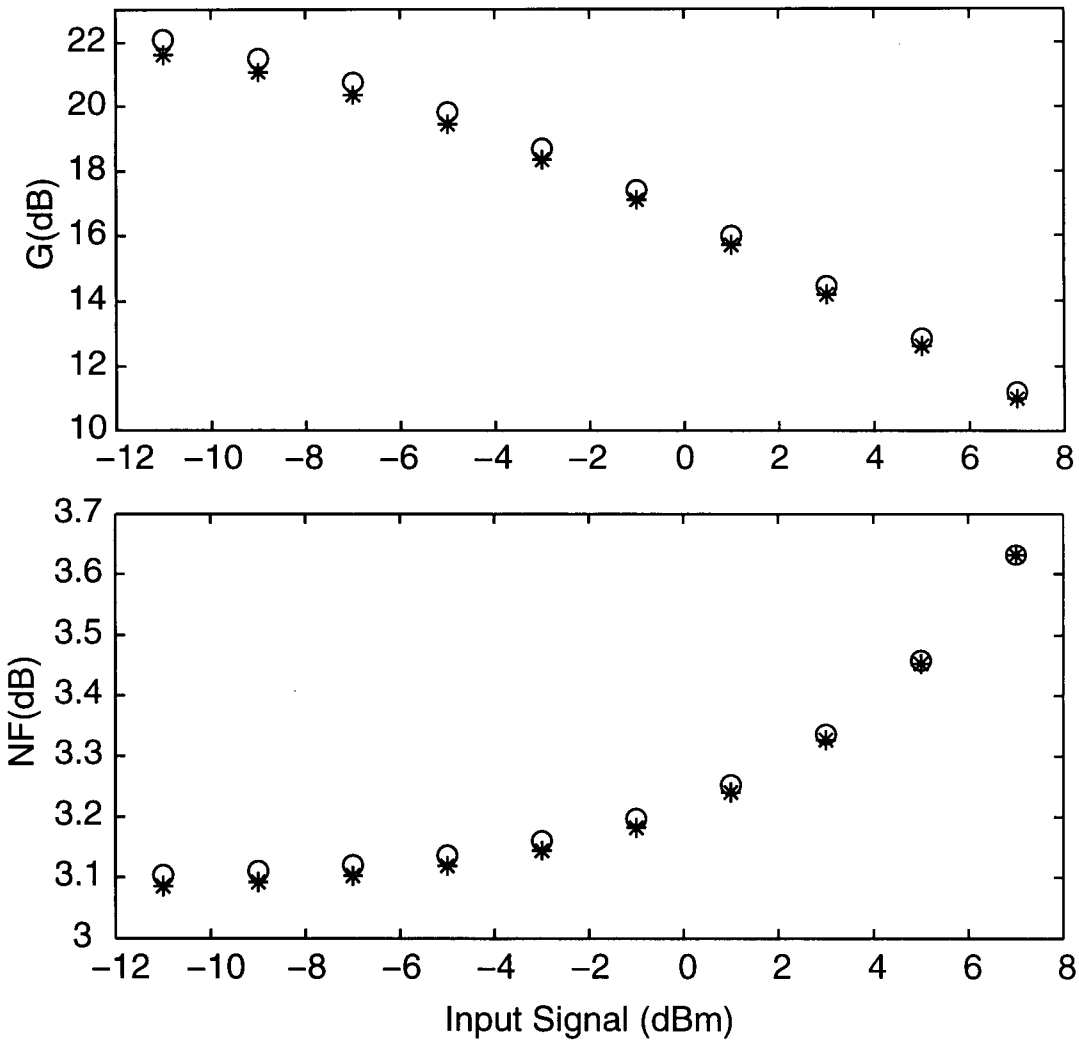

Fig. 3.6: Theoretical comparison between gain and noise figure predictions of the general model (asterisks) with the ones predicted by the proposed model (circles) for the case of EDFA4 with an erbium confinement factor of 1.

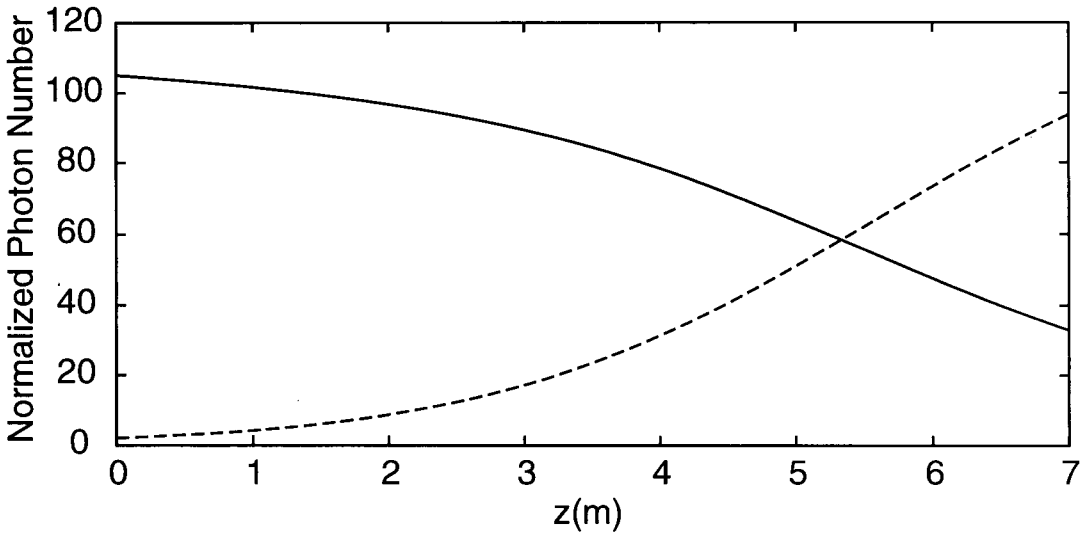

Fig. 3.7: Normalized pump (solid line) and signal (dashed line) photon numbers versus amplifier length for the case of EDFA4 at an input signal power of 0dBm.

EDFA5. It had an estimated erbium confinement factor of 0.7; the signal wavelength was 1551 nm.

Fiber background loss coefficients α_s' and α_p' can be determined by measuring the EDF's absorption coefficient at a wavelength far away from the erbium absorption band. Using the empirical relation for the Rayleigh scattering loss $\alpha_R = C/\lambda^4$ dB/km, where C is a constant [10], [46], the loss at the signal and pump wavelengths can be estimated. The loss coefficient was measured at a wavelength of 1310 nm using the standard cutback method [4] and for EDF5, a loss coefficient of 0.02 dB/m was obtained; consequently the corresponding background loss coefficients are 0.01 and 0.06 dB/m at wavelengths of 1551 and 980nm, respectively. In the standard cutback method, one end of the fiber under test is connected to the signal source and the other end is connected to an optical spectrum analyzer. First, the spectral output power $P_A(\lambda)$ is measured; then a segment of fiber is removed, by cutting away a length, L, of the fiber at its end, and the corresponding optical power spectra $P_B(\lambda)$ is measured again. The fiber loss coefficient, $\alpha(\lambda)$ (in dB per meter), is then calculated from:

$$\alpha(\lambda) = 10 \frac{\log(P_A(\lambda)/P_B(\lambda))}{L} \tag{3.19}$$

The excited state absorption coefficient is traditionally measured using the pump-probe technique [4]-[5]. In this method, a strong pump laser is used to create full population inversion along the EDF under test, and a white light source at the signal wavelength, propagating in the opposite direction of the pump, is used as a probe to measure the ESA coefficient. This measurement technique is difficult as it requires free space optics and careful calibration of the experi-

mental components. Here $\alpha_p' + \alpha_{ESA}$ was measured using the following method. Consider a piece of EDF which is pumped by a 980nm source while the signal is turned off, and the pump source is so strong that near-complete population inversion can be achieved, i.e. N_2 is 1 or close to unity. Under such a situation, equation (3.12) simplifies to:

$$\frac{dP_p}{dz} = -(\alpha_p' + \alpha_{ESA})P_p \tag{3.20}$$

and, therefore, the factor $(\alpha_p' + \alpha_{ESA})$ is equal to the loss of any incremental pump power beyond the pump power at which the complete population inversion has occurred. Accordingly, to obtain the factor $(\alpha_p' + \alpha_{ESA})$ for the EDF5, the transmission of 980nm pump was measured over a 3 m length of fiber at several input pump powers. The upper panel of Fig. 3.8 shows the experimental results of pump loss (Pin/Pout) versus input pump power. In addition, the differential pump loss (ΔPin/ΔPout) was calculated, which is shown in the lower panel of Fig. 3.8. The factor $(\alpha_p' + \alpha_{ESA})$ is equal to the differential loss at high input pump powers, where the near-complete inversion occurs, and was determined to be 0.07 dB/m. This, together with the fact that α_p' is 0.06 dB, shows that excited state absorption at 980nm is very small, in agreement with the results presented in Refs. [4]-[5].

The small signal gain and loss coefficients at the signal and pump wavelengths were determined using the standard cutback method [4]. Measurement of the small signal gain coefficient using the cutback method is similar to loss measurement described above; the only difference is that the input end of the fiber under test is spliced to the output of a 980/1550nm WDM which combines the signal and pump. For this measurement, the pump power should be high enough to

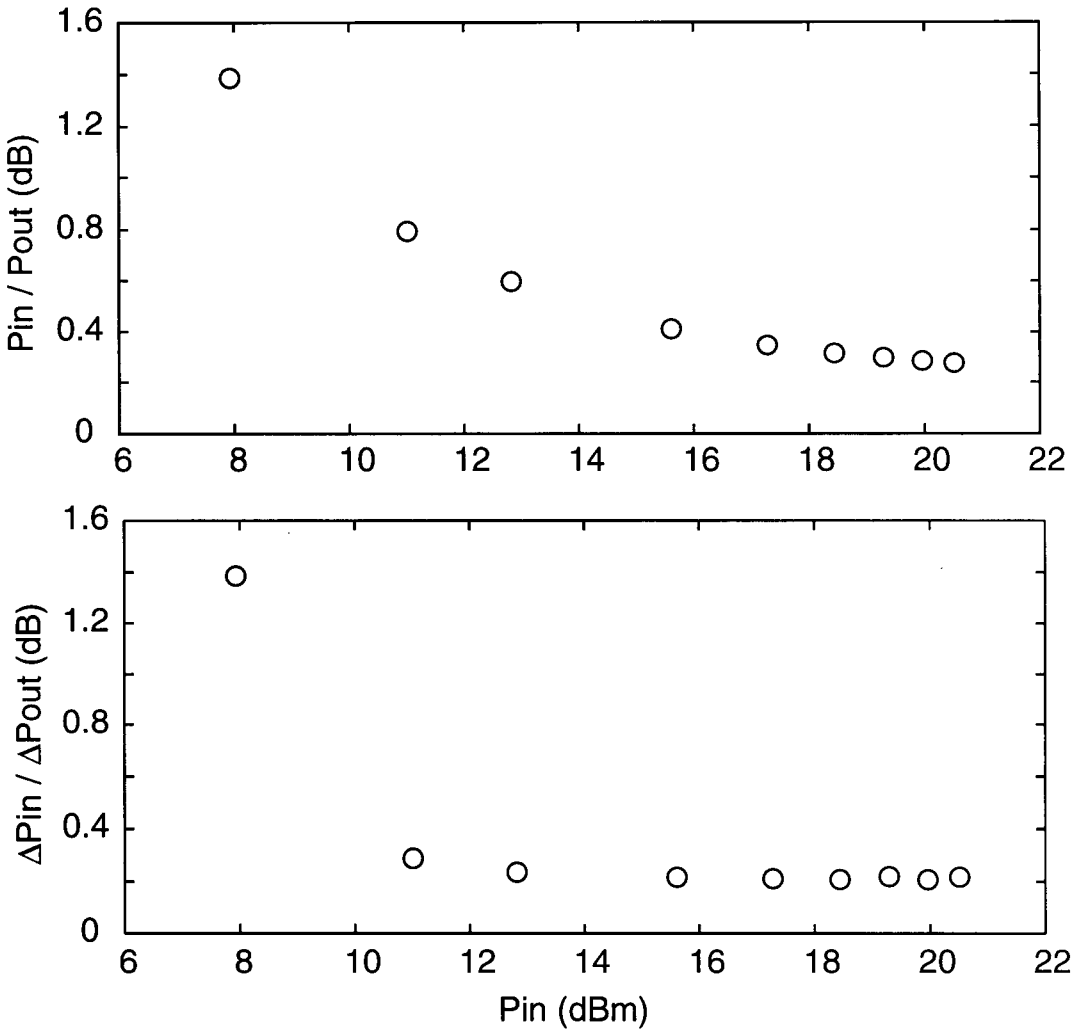

Fig. 3.8: 980nm loss measurement results over 3 m of EDF5. The upper panel shows results of pump loss (pin/pout) versus input pump power and the lower panel shows the differential pump loss (ΔPin/ΔPout) versus input pump power.

create full population inversion along the length of the EDF under test. Due to the presence of the fiber background loss, the cutback method does not provide direct measurement of the gain and loss coefficients, and instead it gives $(g_s - \alpha_s^{'})$, $(\alpha_s + \alpha_s^{'})$ and $(\alpha_p + \alpha_p^{'})$. From cutback measurements and the background loss coefficients given above, g_s, α_s, and α_p were calculated as 2.52 dB/m, 1.89 dB/m, and 2.90 dB/m, respectively.

Next, to compare the predictions of the proposed model versus experimental results, the gain and noise figure of a co-propagating 980-nm-pumped amplifier, EDFA5, were measured versus input signal power ranging from -11 to +7 dBm. EDFA5 was built around 8.94 m of the EDF5, with an input pump power of 144 mW. The EDFA gain was measured, using the optical method described in Section 1.5.1 [10], with an ANDO 6315B optical spectrum analyzer. The EDFA noise figure was measured using the frequency-resolved method described in Chapter 1 at the baseband frequency of 800 MHz using a Rohde&Schwarz FSEA 20 spectrum analyzer. Measurement at 800 MHz together with the fact that the DFB laser signal source had a linewidth of 850kHz ensures that the interferometric noise has negligible effect on the measured noise figure [35]. Also, the presence of an optical bandpass filter at the end of the EDFA makes the contribution of the ASE-ASE beat noise negligible [31]. Therefore, the measured noise figure is primarily due to the signal-ASE beat noise, the same term which gives the theoretical NF, making the comparison between theory and experiment appropriate. Fig. 3.9 shows the results of the comparison; the asterisks show the experimental results and open circles show model predictions. From, Fig. 3.9 it is evident that for both gain and NF, the proposed model is in excellent agreement with the experimental results confirming the theoretical comparison presented in Fig. 3.6.

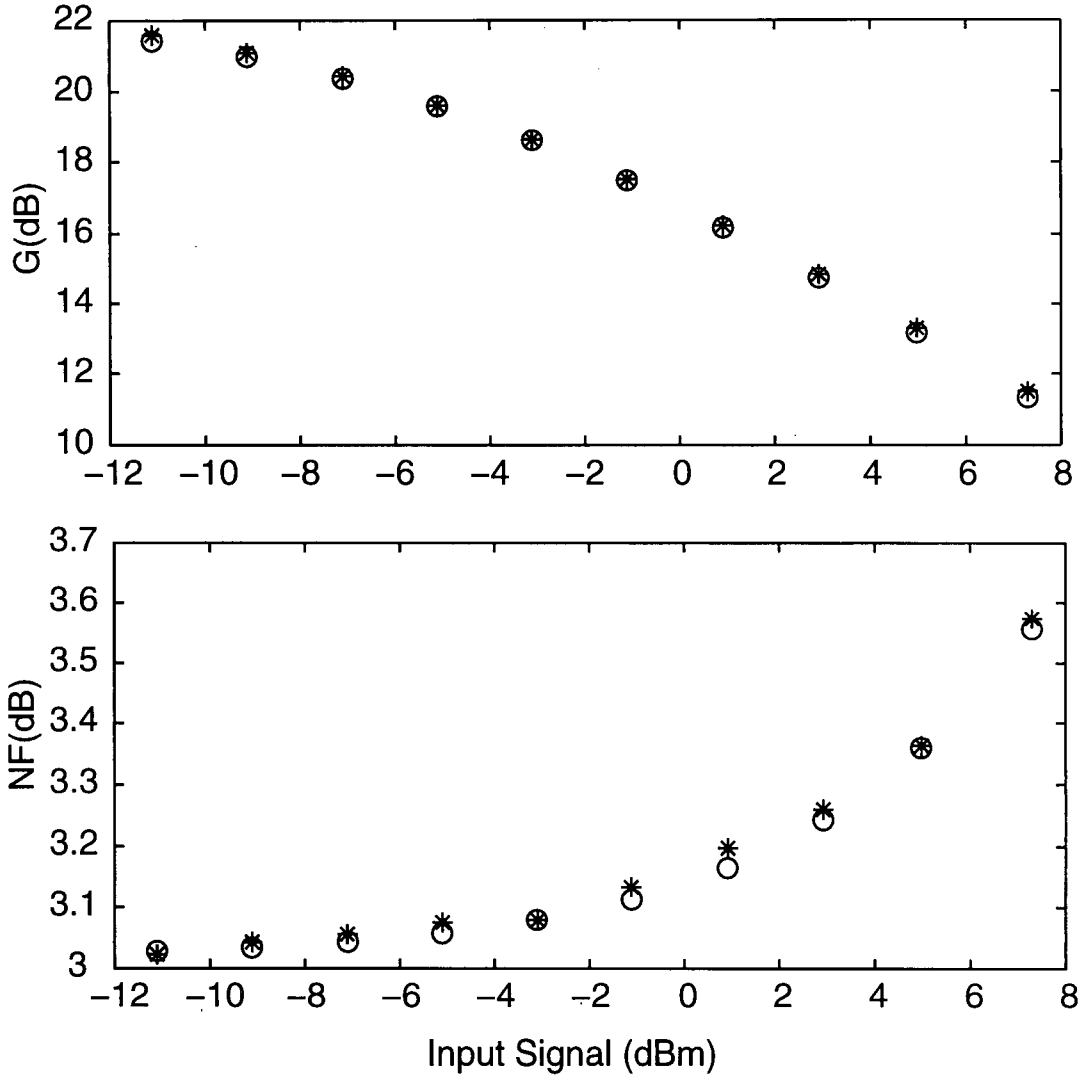

Fig. 3.9: Comparison between measured gain and NF of EDFA5 (asterisks) with the predictions of the proposed model (circles).

3.7 Generalization of the Proposed Model

The focus of the analyses presented so far was on copropagating single-wavelength signal 980-nm-pumped EDFAs, and the applicability of the proposed model was demonstrated for saturated operation. However, from the effective ASE model for multiple signal and pump wavelengths [17], it is easy to show that the proposed model can be extended to include ASE, both 980 and 1480nm pumping, and as many as co- and counter-propagating signals and pumps. Accordingly, the model propagation equations in this general case and for an arbitrary number of k forward propagating (+) and backward propagating (-) signals, pumps and ASE can be written as:

$$\pm\frac{dP_k^{\pm}}{dz} = (\alpha_k + g_k)\, N_2\, P_k^{\pm} + 2\, g_k\, N_2\, h\nu_k\, \Delta\nu_k - \alpha_{ESA}(\nu_k)\, N_2\, P_k^{\pm} - (\alpha_k + \alpha_k')P_k^{\pm} \quad (3.21)$$

$$N_2 = \frac{\sum_k \alpha_k\, P_k^{\pm}/\nu_k}{\sum_k (\alpha_k + g_k) P_k^{\pm}/\nu_k} \quad (3.22)$$

where $\Delta\nu_k$ is zero for signal and pump and for ASE is the frequency interval used in the simulation to resolve the ASE spectrum [17]. This model is also applicable to the case of small signal amplifiers, if the denominator of equation (3.22) is greater than 1, which is satisfied for most practical small-signal amplifiers. This can be explained by considering the fact that the noise performance of small signal amplifiers improves with higher pump powers, and that commercially available pump laser diodes have a typical output power more than 90mW; this amount of pump power is sufficient to justify the assumption made in deriving equation (3.22), making the

proposed model applicable to almost all practical EDFAs.

3.8 Conclusions

In conclusion, using the general rate equation model including background loss at the signal and pump wavelengths, it was shown that the design of efficient saturated EDFAs is achieved by distributing the erbium doping over the entire fiber core, in contrast to generally-accepted design principles. From the radially-dependent rate equation model a simple model was derived which can be used for accurate prediction of gain and NF in saturated EDFAs even with erbium confinement factors as great as 1. Excellent agreement was shown between the gain and noise figure predictions of this model and those of the general rate equation model and also experimental results. A new measurement method was developed which can be used for simple and accurate characterization of excited-state absorption in erbium-doped fibers. Finally, it was shown that the proposed model can be extended to include modeling of a wide variety of 980 and 1480nm pumped EDFAs.

Chapter 4

Dispersion-Induced RIN Degradation and its Impact on 1550nm AM Video Lightwave Transmission Systems

4.1 Introduction

In Chapter 1, the operating principles of 1550nm optically-amplified AM video lightwave transmission systems (CATV systems) were described and it was shown that the performance of such systems is strongly affected by the noise of the different components in these systems. One source of noise in such systems is due to the DFB laser transmitter. In this chapter the effect of fiber dispersion on the relative intensity noise of analog DFB lasers is analyzed theoretically and experimentally and its impact on the overall performance of CATV systems is discussed.

This chapter is organized as follows. In Section 4.2, the motivation of the work presented in this chapter is described. In Section 4.3, the laser RIN measurement technique is described and results of laser RIN measurements versus several lengths of dispersive fibers in frequencies relevant to CATV systems are shown. In Section 4.4, modeling of laser RIN variation with dispersive propagation is described and predictions of the theory are compared with the experimental results. Finally, summary and conclusions of the results presented in this chapter are in Section 4.5.

4.2 Motivation

A stringent requirement for CATV systems is that a high carrier-to-noise ratio (CNR) be maintained along the transmission fiber link. One of the parameters affecting the system CNR is the relative intensity noise (RIN) of the distributed feedback (DFB) laser transmitter. In conventional CNR analysis of analog lightwave transmission systems, it is assumed that the laser RIN remains constant over the transmission fiber link [1], [47]-[48]. However, as shown in Section 1.7, it has been well known that fiber dispersion can affect laser RIN. Nevertheless, there has been no quantitative measure of the degree of laser RIN degradation with fiber dispersion in the frequency range relevant to CATV, nor has there been any discussion of the impact of this effect on overall performance of CATV systems. In this chapter, laser RIN variation with fiber dispersion is carefully analyzed in the frequency range relevant to CATV systems [49]-[50].

4.3 Laser RIN Measurements

In this section, laser RIN measurement technique is described and results of RIN measurements for two analog 1550 DFB lasers versus fiber lengths up to 48 km are presented.

The laser RIN measurement technique used is based on the method developed by Nazarathy, which was described in Section 1.8. However, as discussed in Section 2.3, for achieving higher accuracy, optical power and photodiode responsivity parameters contained in equation (1.18) can be replaced by the photodiode average current, and the resulting equation can be written as:

$$P_N(f) = H(f)\ RIN(f)\ I^2 + 2\,e\,H(f)\,I + P_{th}(f) \tag{4.1}$$

where, *H(f)* is the transfer function of the network connecting the photodiode to the spectrum analyzer, which is equivalent to the factor $(Z^2 B_n)/Z_{in}$ described in Section 2.3.

The RIN measurement setup is shown in Fig. 4.1. It consists of the DFB laser under test, a length of single-mode fiber (SMF), an optical attenuator, a receiver which contains a photodiode and a transimpedance amplifier, an ammeter to measure the average photodiode current, and an RF spectrum analyzer (ESA) which measures the noise power spectral density $P_N(f)$. A series of measurements of $P_N(f)$ and I at various settings of the optical attenuator is made. The RIN spectrum is then obtained from least-squares fit of equation (4.1) to the resulting data at each baseband frequency. This simple "self-calibrating" approach eliminates the need to determine several parameters normally required in conventional RIN measurement technique [10], [16] some of which are difficult to measure accurately, and thereby significantly improves measurement accuracy.

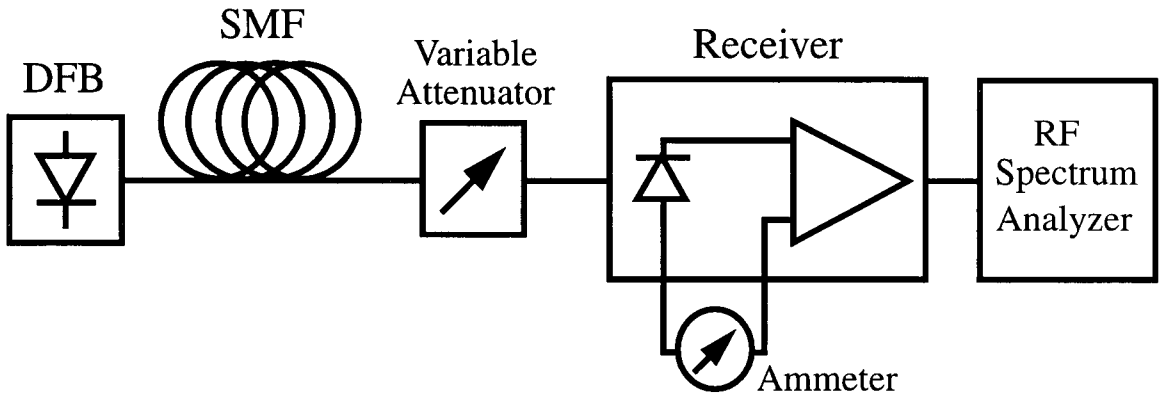

Figure 4.1: Experimental setup for RIN measurement; see text for description.

Fig. 4.2 shows typical raw measurement results at one particular frequency, which is 800MHz in this case. The symbols show measured noise acquired at various settings of the optical attenuator. The solid line shows the quadratic fit, from which the RIN was determined -170.5 dB/Hz. For illustration, the noise power due to the sum of shot and thermal noise is shown by the dashed line; laser RIN is being determined by the difference between the solid and dashed lines. The absolute error in the resulting RIN values depends upon RIN level, which affects the deviation between the quadratic fit and the dashed line, by the accuracy of noise power measurements, and by the accuracy of the average current measurement; accounting for the uncertainties of ± 0.052 dB and ± 0.022 dB for the last two parameters, respectively, the worst-case RIN measurement accuracy is ± 1.5 dB at -172dB/Hz.

Using the above technique the RIN of two analog DFB lasers, DFB1 and DFB2, were measured for several lengths of standard single mode fiber. In all cases, the launched power into the fiber was kept below 4.5 dBm to avoid nonlinear effects. Fig. 4.3 shows frequency-resolved measurements of the RIN of DFB1 at the laser, indicated as 0km, and after 32 and 48km of standard single-mode fiber. At 0 km the laser RIN is quite low; the slight increase with frequency reflects the beginning of the large increase in RIN seen at the relaxation oscillation frequency, which is much higher than the range of frequencies shown in Fig. 4.3. After fiber propagation, two effects are apparent: the first is seen at low frequencies, where the RIN has increased because of the interferometric noise caused by double Rayleigh scattering in the transmission fiber. This effect has been extensively studied [51]-[52], and will not be considered here. The second effect seen in Fig. 4.3 at higher frequencies, is an increase in RIN with fiber length; for a

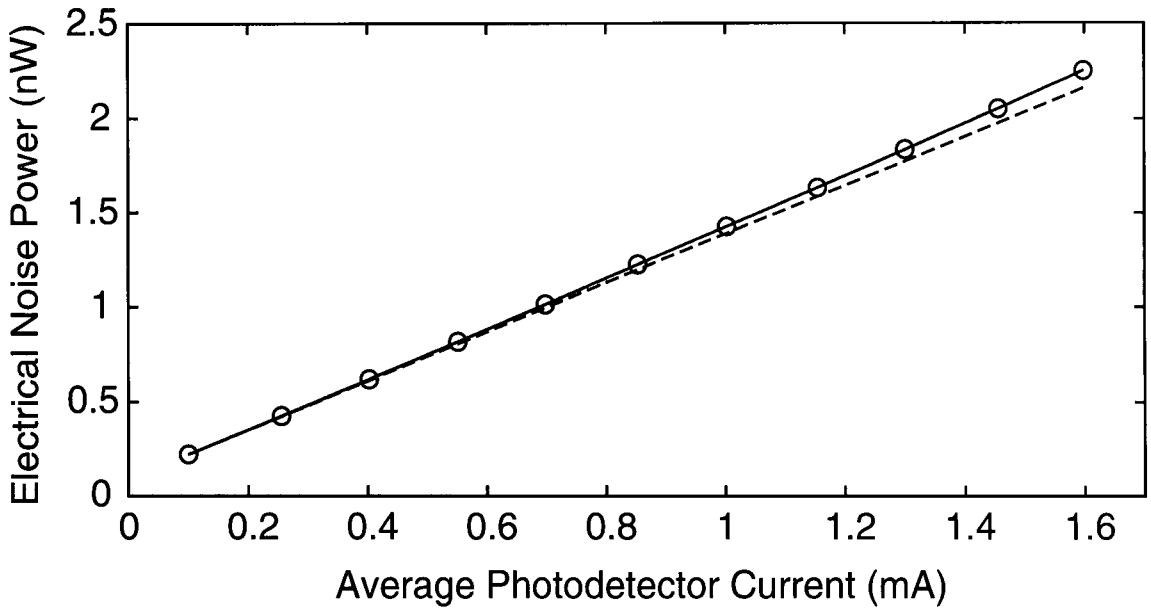

Figure 4.2:Typical measured electrical noise power versus average photodiode current, for a baseband frequency of 800MHz. The open symbols show the measured results, the solid line is the quadratic fit discussed in the text, and the dashed line shows the noise power due to the sum of shot and thermal noise. The RIN value is determined to be -170.5 dB/Hz from these data.

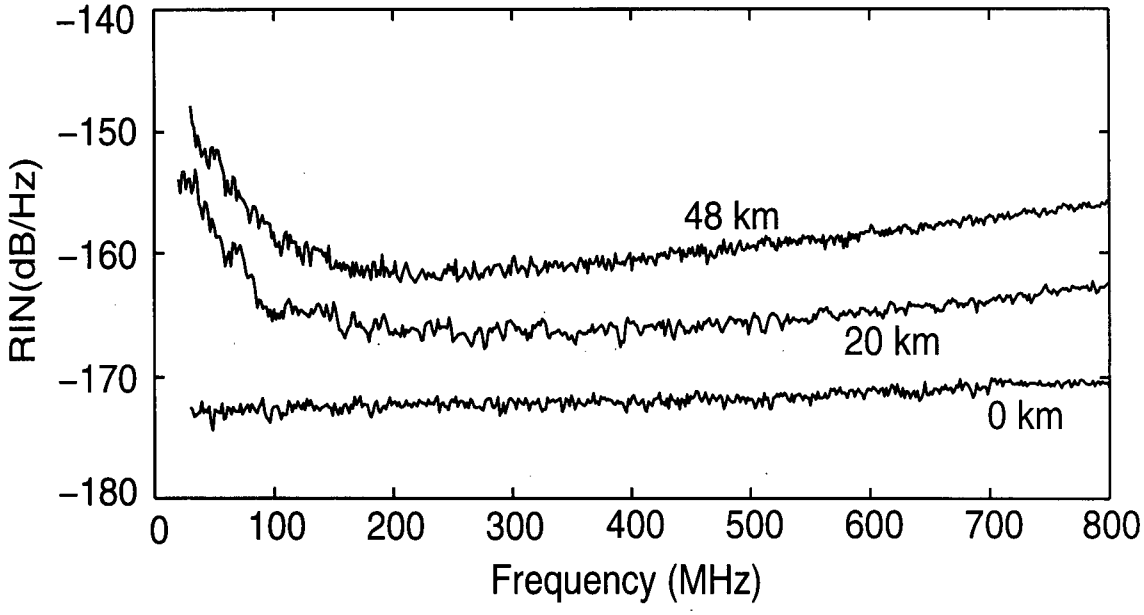

Figure 4.3: Frequency-resolved RIN for DFB1 at fiber lengths of 0, 20, and 48km.

particular fiber length this degradation increases with increasing frequency. Therefore, the impact of this effect will be greatest on the higher frequency channels. From Fig. 4.3 it is apparent that, after 48km of fiber RIN has been degraded by 15dB at 800MHz.

To more clearly show the distance dependence, in Fig. 4.4 the measured RIN as a function of fiber length is shown. The open circles in Figs. 4.4(a) and (b) show results for DFB1 and DFB2, respectively, at the baseband frequency of 800MHz. For both lasers RIN increases substantially and has a similar form; the degree of degradation is less for DFB2. As will be shown later, the lasers have linewidths less than 1MHz, which ensures that the noise due to fiber double Rayleigh scattering has a negligible effect on the measured RIN at 800MHz [51] and therefore the RIN degradations shown in Fig. 4.4 are solely due to the phase to intensity noise conversion.

4.4 Modeling and Discussion

As described in Section 1.7, modeling of laser RIN variation due to fiber dispersion has been already accomplished. The comprehensive modeling approach is based on the model developed by Marshall et. al. [29] which considers the coherent addition of the intrinsic RIN with the PM-to-AM converted RIN. However, this model is involved and requires knowledge of several laser parameters, some of which can be challenging to measure accurately. Given that analog DFB lasers demonstrate low intrinsic RIN at frequencies relevant to CATV (as shown in Fig. 4.3), and that in CATV systems the fiber link is generally longer than 40km, the coherent effects described by Marshall et. al. can be ignored and laser RIN after dispersive propagation can be calculated by an incoherent addition of laser intrinsic AM noise and PM-to-AM converted noise;

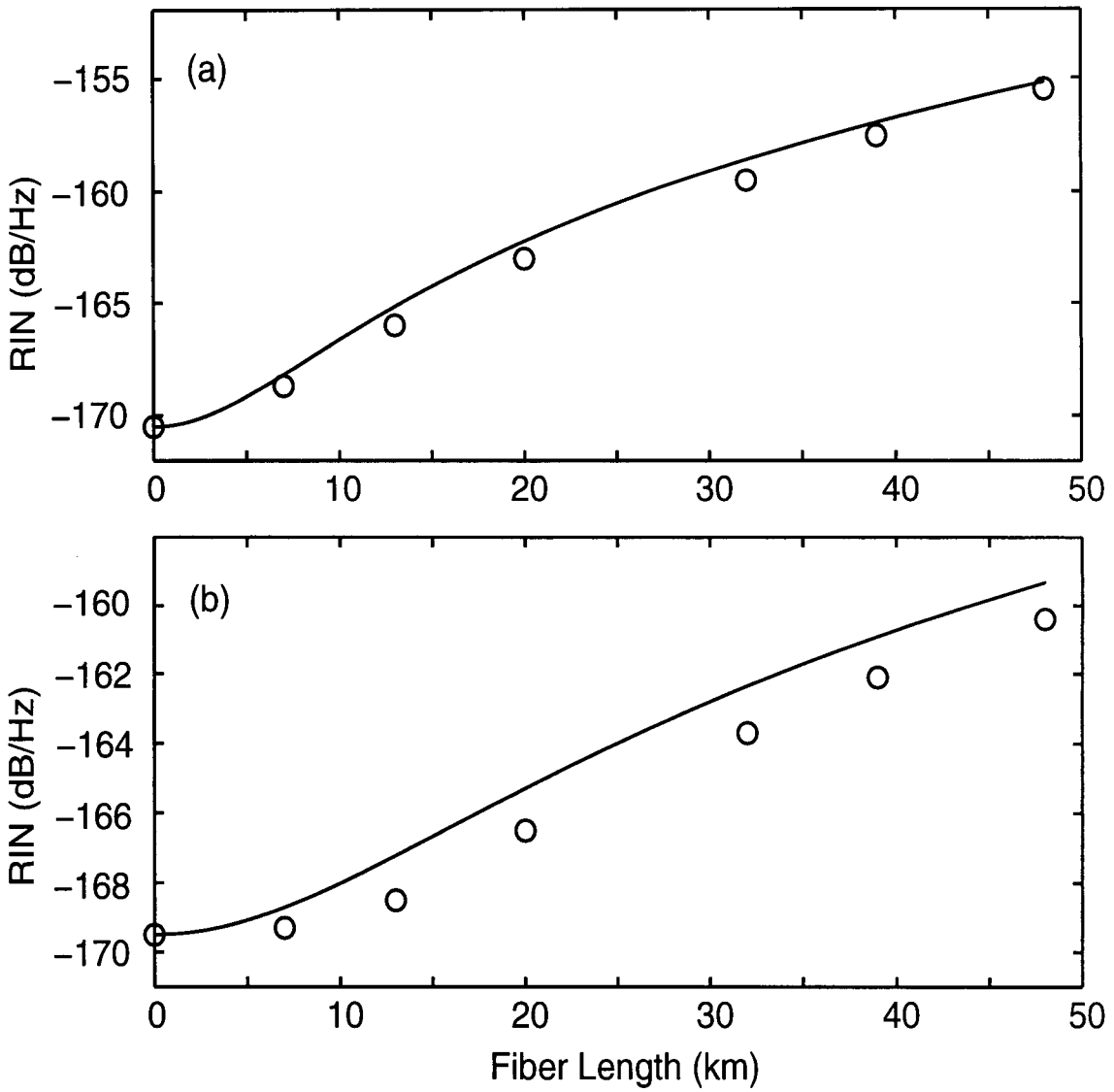

Figure 4.4:RIN versus fiber length (a) for DFB1 and (b) for DFB2. Open circles show measured results, and the solid curves show the RIN calculated using equation 4.3 and the measured intrinsic RIN.

as will be shown this greatly simplifies the analysis. The RIN degradation ΔRIN due to PM-to-AM noise conversion mediated by fiber dispersion can then be obtained from the simplified model by Yamamoto et. al. [28], described in Section 1.7, and is given by,

$$RIN(f) = \frac{1}{2}\left(\sum_{n=0}^{\infty} 4 J_n\left(\frac{1}{f}\sqrt{\frac{2\,\Delta\nu\,\Delta f}{\pi}}\right) J_{n+1}\left(\frac{1}{f}\sqrt{\frac{2\,\Delta\nu\,\Delta f}{\pi}}\right) \sin\left\{\frac{(2n+1)}{c}\pi f^2\lambda^2 DL\right\}\right) \quad (4.2)$$

where J_n is the Bessel function of the first kind, $\Delta\nu$ is the laser linewidth, Δf is the frequency interval over which RIN is calculated and is equal to 1Hz, λ is the laser wavelength, D is the fiber dispersion, L is the fiber length, and c is the velocity of light in vacuum. For cases that $\frac{1}{f}\sqrt{\frac{2\,\Delta\nu\,\Delta f}{\pi}} \leq 0.01$, which is always satisfied for the range of frequencies relevant to CATV, equation 4.2 can be well approximated by

$$\Delta RIN(f) = \frac{4\,\Delta\nu}{\pi f^2} \sin^2(\pi f^2\lambda^2 DL/c) \; . \quad (4.3)$$

The significance of equation (4.3) is that it is only required to know the laser linewidth and wavelength to characterize the laser and to calculate laser RIN degradation with fiber dispersion.

Now comparison of the predictions of equation (4.3) with the experimental results is considered. To determine the linewidths of the two lasers, the modulation sideband technique was used [10],[53]. With this method, the linewidth measurement can be performed at an intermediate frequency, overcoming the low frequency limitation of the detection electronics. In this technique, the laser diode current is directly modulated by small sinusoidal signals, creating sidebands

around the carrier; a delayed self-homodyne technique is used to mix the carrier with the side-bands; the laser linewidth is then obtained from the detected signal which contains the laser line shape at the modulating frequency. The experimental setup for the linewidth measurement is shown in Fig. 4.5. The measurement setup consists of the laser under test, a signal generator for direct modulation of the laser DC current, a variable attenuator for adjusting the optical signal power, an interferometer, a receiver and an RF spectrum analyzer. The interferometer consists of two couplers, 7km of SMF fiber as a delay line, and a polarization controller for adjusting the level of the detected electrical signal. The receiver and ESA are the same as ones used in the RIN measurement setup. The modulation frequency was 200MHz and the ESA resolution bandwidth was 10kHz. Fig. 4.6 shows the experimental results for the two lasers tested. the dotted curves show the measured spectrum of the two lasers around the modulating frequency; the solid lines are the Lorentzian fits used to obtain the laser linewidth and yielded linewidths of 850 and 310 kHz for DFB1 and DFB2, respectively. The accuracy of these linewidth measurements are estimated to be approximately $\pm 10\,\%$.

Inserting the measured linewidth value in equation (4.3), the RIN was calculated as a function of distance by combining the measured laser intrinsic RIN and the calculated RIN degradation, ΔRIN. Results are shown by the solid lines in Fig. 4.4; the fiber dispersion D was taken to be 17 ps/nm-km and the measured laser wavelengths of 1552 and 1547 nm were used for DFB1 and DFB2, respectively. Given that the ΔRIN is incoherently combined with the laser intrinsic RIN, the predicted RIN represents the upper limit. Nevertheless, as can be seen from Fig. 4.4 there is an excellent agreement between the estimated RIN and the experimental results, with the

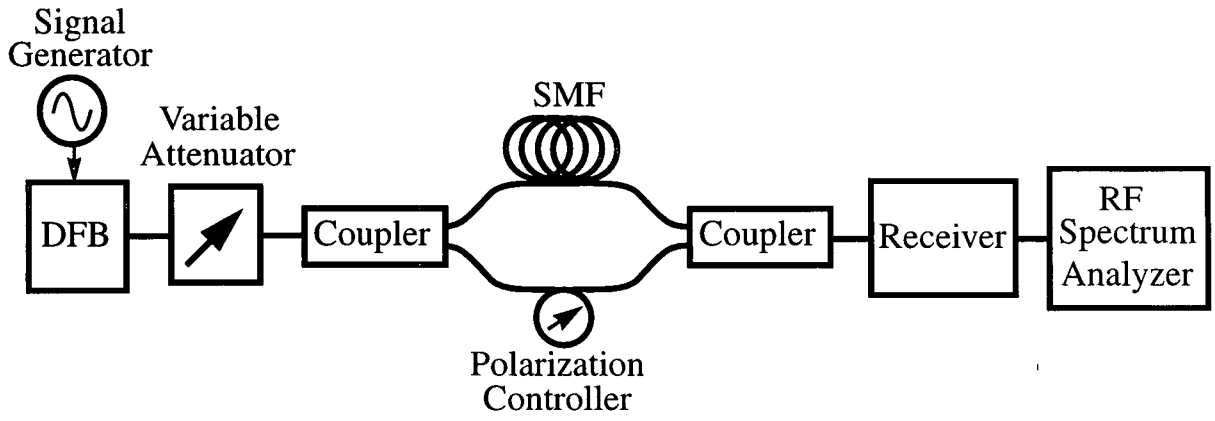

Figure 4.5: Experimental setup for linewidth measurement; see text for description.

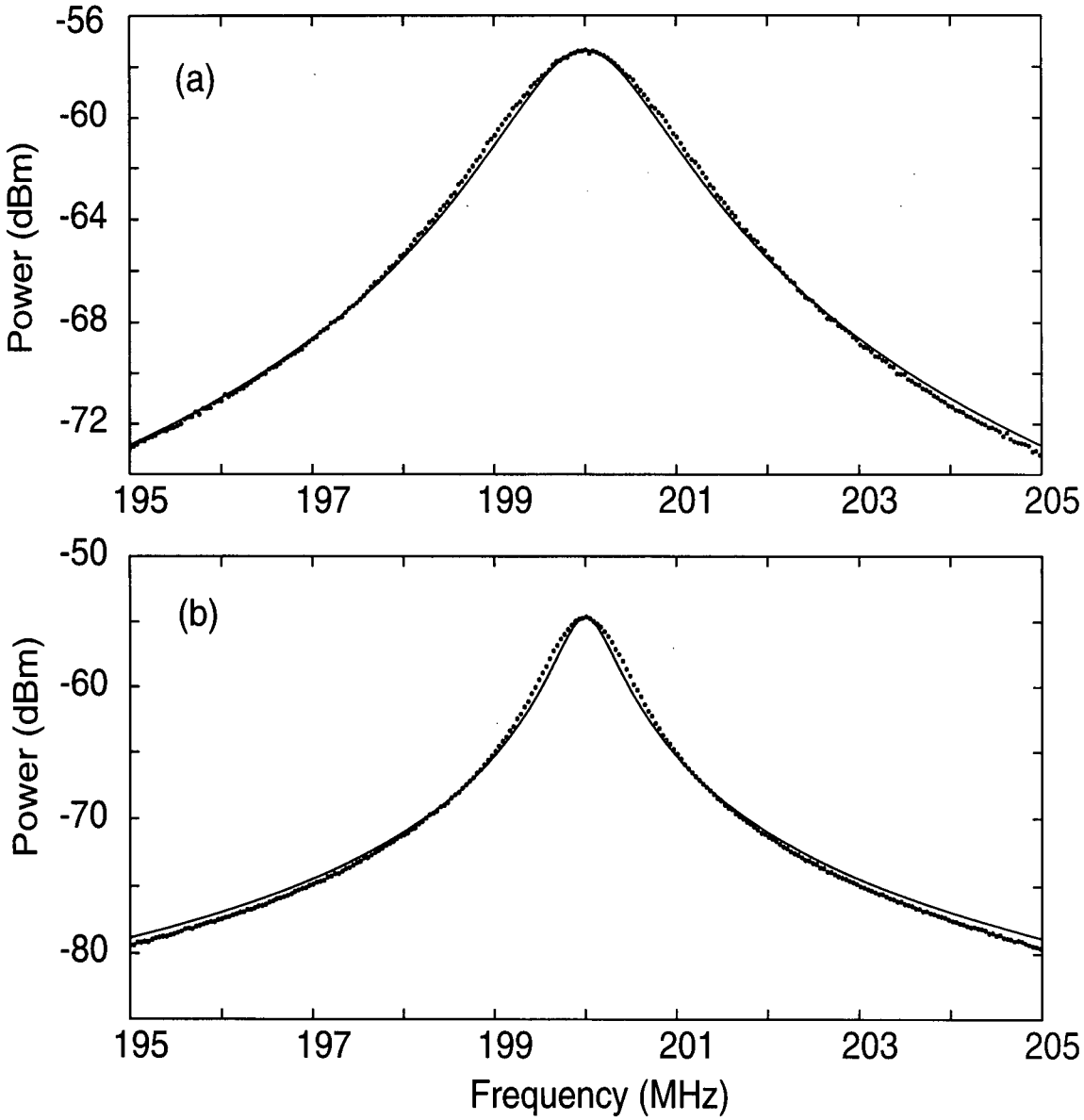

Figure 4.6:Measured laser spectrum and the Lorentzian fit for laser linewidth measurement (a) for DFB1 and (b) for DFB2. The dotted curves are the experimental results and the solid curves are the Lorentzian fits which yield linewidths of 850 and 310kHz for DFB1 and DFB2, respectively.

predicted values lying slightly higher than the measured ones, as expected. This suggests that for DFB lasers demonstrating low intrinsic RIN on the order of -170dB/Hz, which is typical for analog 1550nm DFB lasers, the simplified theory adopted is appropriate and can give an accurate estimate of the laser RIN degradation by dispersive propagation.

All analyses of overall CATV system CNR presented to date have assumed the laser RIN unaffected by fiber propagation, which is substantially in error, as shown above. To assess the impact of the RIN degradation on typical CATV systems, CNR calculations are performed for two representative 1550nm optically-amplified AM video transmission systems: the first, which is called System A, incorporates one erbium-doped fiber amplifier (EDFA) as a power amplifier and has a link length of 60km; the second, System B, has a 120km fiber link and includes a power amplifier and an in-line amplifier. For AM-VSB video lightwave systems with an EDFA, the AM CNR can be written as [1], [48]

$$CNR = \frac{P_{signal}}{N_{RIN} + N_{shot} + N_{thermal} + N_{EDFA}}. \tag{4.4}$$

As described in Refs. [1], [48], the signal power is given by

$$P_{signal} = (m R P_{RX})^2/2,$$

the thermal noise by

$$N_{thermal} = n^2 B_e,$$

the shot noise by

$$N_{shot} = 2\,e\,R\,P_{RX}\,B_e,$$

and the EDFA noise by

$$N_{EDFA} = (2\,h\nu\,(NF - (1/G)))/P_{in} \quad .$$

However, in contrast with previous analyses, the RIN noise must be described by

$$N_{RIN} = (RIN_{int} + \Delta RIN)\,B_e\,R^2\,P_{RX}^2 \ ,$$

where the additional parameter ΔRIN is introduced, to describe the effect of laser RIN degradation caused by fiber dispersion. In the above equations, m is the peak AM modulation depth per channel, R is the photodiode responsivity, P_{RX} is the received optical power, RIN_{int} is the laser intrinsic relative intensity noise measured at the laser output, B_e is the bandwidth of each video channel, and n is the receiver equivalent thermal noise current. NF, G, and P_{in} are the EDFA noise figure, gain and optical input power respectively. System parameters used in the calculations are given in Table 4.1, which are typical values for conventional CATV systems. The calculation results are shown in Fig. 4.7 (a) and (b) for systems A and B, respectively; the dashed lines show the conventional results where ΔRIN is neglected, and the solid lines show the results including RIN degradation for three different laser linewidths of 0.5, 1, and 1.5 MHz, as indicated. The results clearly show that laser RIN degradation caused by fiber dispersion can significantly impair CNR performance of the CATV systems; this impairment is most severe at higher baseband frequencies and can be several dB for the system parameters shown in Table 4.1.

TABLE 4.1: Parameters used in the CNR calculations of System A and System B

Parameters	Value
Peak AM Modulation Index, m	3%
Photodiode Responsivity, R (A/W)	0.9
Receiver Input Power, P_{RX} (dBm)	0
Laser Intrinsic RIN, RIN_{int} (dB/Hz)	-170
Bandwidth of Each Channel, B_e (MHz)	4
Receiver Equivalent Noise Current, n $((pA/\sqrt{Hz}))$	7
EDFA Noise Figure, NF (dB)	5
EDFA Optical Gain, G (dB)	13
EDFA Optical Input Power, P_{in} (dBm)	4

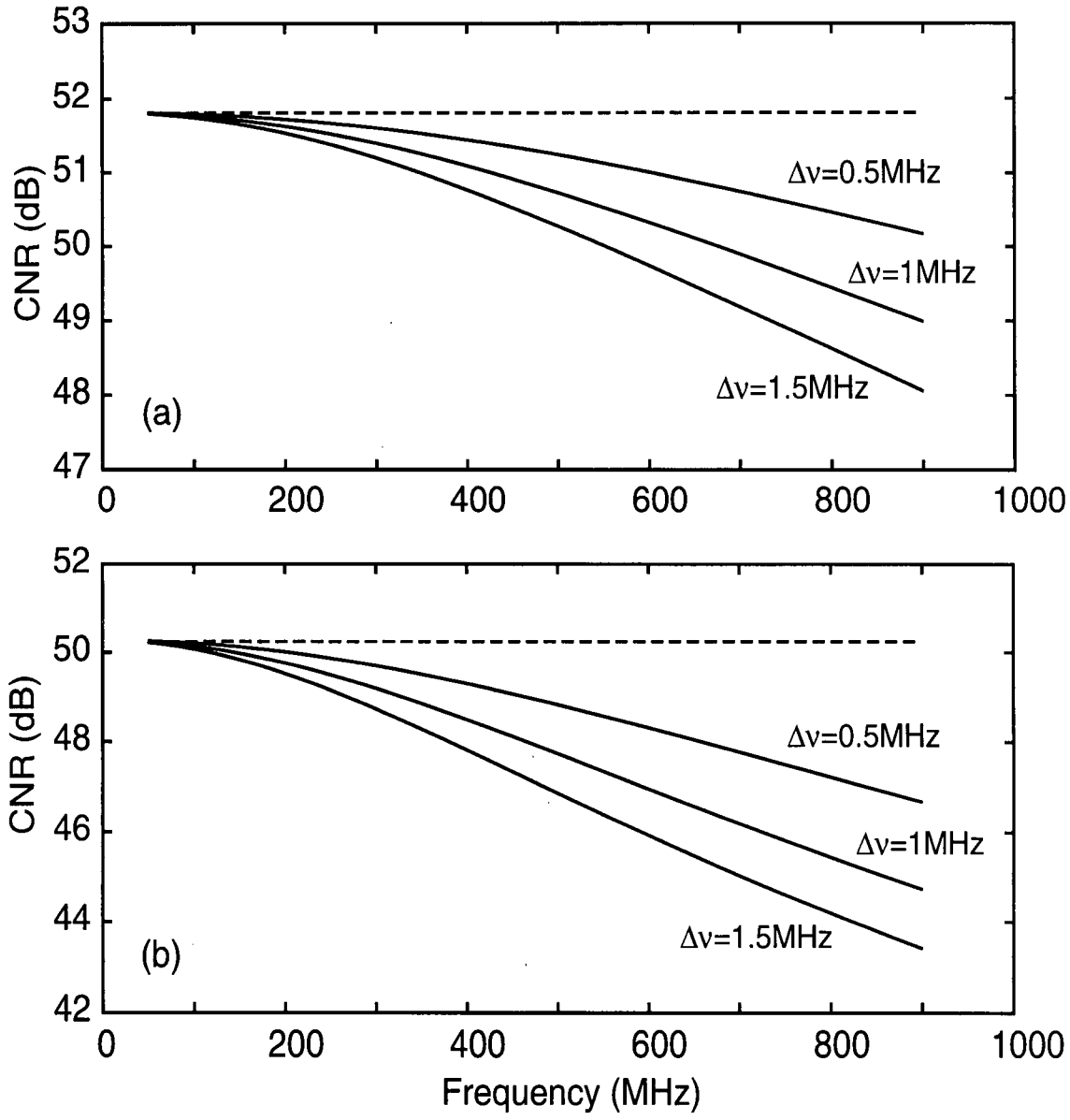

Figure 4.7:CNR versus frequency calculated for (a) System A, and (b) System B. Dashed lines show the conventional analysis. Solid lines include RIN degradation for linewidths of 0.5, 1, and 1.5 MHz, as indicated.

In the analyses presented above only linear fiber propagation was considered. This is because the objective of the work presented here was to study only the effect of fiber dispersion. However, in practical CATV systems, the optical power launched into the transmission fiber can be as large as 18dBm, and therefore fiber nonlinearity becomes important. However, a recent theoretical study by Cartaxo et. al. [54] has shown that for frequencies less than 3GHz, fiber nonlinearity has no effect on the laser phase to intensity noise conversion. However, it would be interesting to investigate this issue experimentally in future research work.

4.5 Summary and Conclusions

A sensitive self-calibrating technique for laser RIN measurements was described. Using this technique, the RIN of two analog 1550nm DFB lasers were measured and for the first time, RIN values as low as -172 dB/Hz were reported for analog DFB lasers. The RIN of the two lasers were also measured, in the frequency range relevant to CATV systems, for several lengths of standard single-mode fiber. The measurements show that laser RIN increases with increasing frequency and fiber length, and that this degradation is a function of laser linewidth. The measurement results are in close agreement with a simple theory which only requires knowledge of laser linewidth to calculate the RIN degradation. The effect of laser RIN degradation by dispersive propagation on the CNR performance of two analog CATV systems was analyzed theoretically, and shown that it can severely impair the CNR of these systems. It is especially important in the case of long distance CATV systems to account for the effects of RIN degradation, and for optimal CNR, analog lasers should be chosen on the basis of both RIN and linewidth.

Chapter 5

Summary and Conclusions

In Chapter 2, a simple electrical measurement technique for characterization of EDFA noise figure was presented. This technique is built upon equation (2.12), which relates the EDFA noise figure to five parameters which can be measured easily and with high accuracy. An absolute accuracy of ± 0.3 dB was achieved for the electrical NF measurements presented, which is significantly better than conventional RIN subtraction results reported to date. For optical noise figure measurements, the accuracy of the conventional polarization nulling technique was enhanced by introducing a simple calibration technique; this technique allows accurate determination of the loss incurred by the polarizer and the polarization controller used in the measurement setup. For the case of two copropagating 980nm pumped EDFAs, an excellent agreement was shown between the optical and electrical noise figure measurements in saturation. This results are in contrast to earlier reports [13]-[14], by Willems and van der Platts, where significant differences between the two measurements have been observed for the case of an EDFA similar to ones used in the work presented in Chapter 2. Reports by Willems and van der Platts caused a great deal of controversy and excitement, as they were claiming: first, that it is possible to achieve significant reduction of EDFA noise figure in saturation; second, that the conventional semi-classical models are not applicable to EDFAs operating in saturation; and third, that

optical noise figure measurements were inappropriate and unreliable. The careful establishment of high accuracy in both electrical and optical noise figure measurements described in Chapter 2, and excellent agreement obtained between the two measurement approaches, strongly suggests that the first two of the conclusions of Ref. [13]-[14], outlined above, are incorrect. The conclusion concerning an appropriate measurement approach for EDFA noise figure characterization is that the electrical method proposed in Chapter 2 is much simpler and can provide more accurate results compared to commonly used optical measurement techniques; it seems reasonable to expect widespread adoption of electrically-based noise measurement techniques for EDFA noise figure characterization.

In Chapter 3, using a general, radially dependent rate-equation model it was shown that amplified spontaneous emission has negligible effect on the gain and noise performance of a signal-saturated EDFA having an erbium confinement factor of one. This, coupled with the fact that erbium-doped fibers have rather large background losses at the signal and pump wavelengths, and that for a given amplifier the required EDF length increases with erbium confinement, leads one to the conclusion that, in contrast to the generally-accepted design principles, saturated EDFAs with non-confined EDFs would have better performance compared to ones with confined EDFs. Using the general model, it was shown that the gain of a typical 980nm pumped EDFA can be upgraded from 16.73 to 17.72dB if the EDF confinement factor is changed from 0.5 to 1. It was shown that the widely accepted Saleh model cannot accurately predict the gain and noise figure performance of EDFAs containing non-confined EDFs. This was attributed to the fact that the derivation of this model has been based on the principle assumption that the

erbium is confined near the center of fiber core. From the general model, a simplified one-dimensional steady-state model was derived which can accurately predict gain and noise figure of both confined and non-confined saturated EDFAs. In this model, the relatively hard to measure intrinsic saturation powers, normally contained in the conventional models, were eliminated without compromising accuracy; this simplification is equivalent to assuming that the spontaneous emission lifetime is infinity, which physically means that the spontaneous emission has no impact on the population inversion of the system. The proposed model contains only small signal gain and loss coefficients which can be measured easily and with high accuracy. Finally it was shown that the proposed model, can be extended to include modeling of almost all practical EDFAs.

In Chapter 4, an enhanced measurement method for simple and accurate characterization of laser RIN was described, and RIN values as low as -172 dB/Hz were shown for an analog 1550nm DFB laser. This is the lowest RIN value ever reported, and it is significantly lower than the normally reported values for analog 1550nm DFB lasers, which are in the order of -155 dB/Hz. Measurement results for RIN of two analog DFB lasers were shown for several lengths of standard single mode fibers up to 48 km, and in the frequency range relevant to CATV systems for the case of linear propagation. The results show that laser RIN increases with increasing frequency and fiber length. These results are in contrast to conventional CNR analysis of CATV systems where it is assumed that laser RIN remains constant over the entire fiber transmission link. This degradation was attributed to the well known laser phase to intensity noise conversion by dispersive propagation. For the particular case of CATV systems, it was shown that, instead

of using the complex model of Marshall et. al., the simplified model of Yamamoto et. al. is sufficiently accurate for predicting RIN degradation of DFB lasers due to fiber dispersion. The particular advantage of this model is that it contains only laser linewidth as the laser parameter. Finally, theoretical results of the effect of laser RIN degradation by dispersive propagation on the CNR performance of two analog CATV systems were presented. These results show that, even in optically-amplified CATV systems, RIN degradation by fiber dispersion can severely impair CNR performance of CATV systems, and for achieving optimal CNR performance of CATV systems, analog lasers should be chosen on the basis of both RIN and linewidth.

Bibliography

[1] H. Dai, S. Ovadia, and C. Lin, "Hybrid AM-VSB/M-QAM multichannel video transmission over 120-km of standard single-mode fiber with Er-doped fiber amplifiers," *IEEE Photon. Technol. Lett.*, vol. 8, no. 12, pp. 1713-1715, 1996.

[2] A. Bjarklev, *"Optical Fiber Amplifiers: Design and System Applications,"* Artech House, Boston, MA, 1993.

[3] P. C. Becker, N. A. Olsson, and J. R. Simpson, *"Erbium-doped fiber amplifiers: fundamentals and technology,"* Academic Press, San Diego, CA, 1999.

[4] E. Desurvire, *"Erbium-Doped Fiber Amplifiers,"* John Wiley & Sons, New York, 1994.

[5] R. I. Laming, S. B. Poole, and E. J. Tarbox, "Pump excited-state absorption in erbium-doped fibers," *Opt. Lett.*, vol. 13, no. 12, pp. 1084-1086, 1988.

[6] M. Tachikura, "Numerical calculation of multiple reflected optical power in optical fiber transmission lines," *IEEE Photon. Technol. Lett.,* vol. 6, No. 1, pp. 109-111, 1994.

[7] C. Hentschel, E. M. Muler, and E. Leckel, "EDFA noise figure measurements - Comparison between optical and electrical technique," Hewlett Packard, Boblingen Instruments Division, in *1994 Lightwave Symp.*

[8] S. Poole, "Noise Figure Measurement in Optical Fibre Amplifiers," in *Symposium on Optical Fiber Measurements,* 1994, NIST Special Publication 864 (National Institute of Standards and Technology, Boulder, CO, 1994), pp. 1-6.

[9] J. Aspell, J. Federici, B. Nyman, D. Wilson, and D. Shenk, "Accurate noise figure measurements of erbium-doped fiber amplifiers in saturation conditions," in *Optical Fiber Communication Conference,* vol. 5, 1992, OSA Technical Digest Series (Optical Society of America, Washington, D.C., 1992), pp. 189-190.

[10] D. Derickson, "*Fiber optic test and measurement*," Hewlett-Packard Company, Prentice-Hall, NJ, 1998.

[11] K. Bertilsson, P. Andrekson, and B. Olsson, "Noise Figure of Erbium Doped Fiber Amplifiers in the Saturated Regime," *IEEE Photon. Technol. Lett.*, vol. 6, No. 2, pp. 199-201, 1994.

[12] T. Kashiwada, M. Shigematsu and M. Nishimura, "Accuracy of noise figure measurement for erbium-doped fiber amplifiers by the optical method," *Technical Digest Symposium on Optical Fiber Measurements, 1992,* National Institute of Standards and Technology Special Publication 839, pp. 209-212.

[13] F. Willems and J. van der Plaats, "EDFA noise-figure reduction in the saturated operation regime," in *Optical Fiber Communication Conference,* vol. 8, 1995, OSA Technical Digest Series (Optical Society of America, Washington, D.C., 1995), pp. 44-45.

[14] F. Willems and J. van der Plaats, "Experimental Demonstration of Noise Figure Reduction Caused by Nonlinear Photon Statistics of Saturated EDFA's," *IEEE Photon. Technol. Lett.*, vol. 7, No. 5, pp. 488-490, 1995.

[15] F. Willems, J. van der Plaats, C. Hentschel, and E. Leckel, "Optical amplifier noise figure determination by signal RIN subtraction," in *Symposium on Optical Fiber Measurements,* 1994, NIST Special Publication 864 (National Institute of Standards and Technology, Boulder, CO, 1994), pp. 7-9.

[16] Product Note 71400-1, "Lightwave Signal Analyzers Measure Relative Intensity Noise," Hewlett Packard Publication, 1996.

[17] C. Giles and E. Desurvire, "Modeling erbium-doped fiber amplifiers," *J. Lightwave Technol.*, vol. 9, pp. 271-283, 1991.

[18] C. Barnard, P. Myslinski, J. Chrostowski, and M. Kavehrad, "Analytical models for rare-earth-doped fiber amplifiers and lasers," *J. Lightwave Technol.*, vol. 30, no. 8, pp. 1817-1830, 1994.

[19] A. Saleh, R. Jopson, J. Evankow, and J. Aspell, "Modeling of gain in erbium-doped fiber amplifiers," *IEEE Photon. Tech. Lett.,* vol. 2, no. 10, pp. 714-717, 1991.

[20] R. Jopson and A. Saleh, "Modeling of gain and noise in erbium-doped fiber amplifiers," *SPIE Vol. 1581 Fiber Laser Sources and Amplifiers III,* pp. 114-119, 1991.

[21] I. Habbab, A. Saleh, N. Frigo, G. Bodeep, "Noise Reduction in Long-Haul Lightwave All-Amplifier Systems," *J. Lightwave Technol.,* vol. 10, No. 9, pp. 1281-1289, 1992.

[22] Y. Sun, A. K. Srivastava, J. L. Zyskind, J. W. Sulhoff, C. Wolf and R. W. Tkach, "Fast power transients in WDM optical networks with cascaded EDFAs," *Electron. Lett.,* vol. 33, no. 4, pp. 313-314, 1997.

[23] E. Ḋesurvire, "An explicit analytical solution for the transcendental equation describing saturated erbium-doped fiber amplifiers," *Optical Fiber Technology,* no. 2, pp. 367-377, 1996.

[24] Y. Sun, G. Luo, J. L. Zyskind, A. A. M. Saleh, A. K. Srivastava, and J. W. Sulhoff, "Model for gain dynamics in erbium-doped fiber amplifiers," *Electron. Lett.,* vol. 32, no. 16, pp. 1490-1491, 1996.

[25] Y. Sun, J. L. Zyskind, and A. K. Srivastava, "Average inversion level, modeling, and physics of erbium-doped fiber amplifiers," *IEEE J. Sel. Top. Quantum. Electron.*, vol. 3, no. 4, pp. 991-1007, 1997

[26] A. Bononi and L. A. Rusch, "Doped fiber amplifier dynamics: a system perspective," *J. Lightwave Technol.,* vol. 16, no. 5, pp. 945-957, 1998.

[27] F. Lai, C. Liu and J. Jou, "Analyses of distortions and cross modulations in erbium-doped fiber amplifiers," *IEEE Photon. Tech. Lett.,* vol. 11, no. 5, pp. 545-547, 1999.

[28] S. Yamamoto, N. Edagawa, H. Taga, Y. Yoshida, and H. Wakabayashi, "Analysis of laser phase noise to intensity noise conversion by chromatic dispersion in intensity modulation

and direct detection optical-fiber transmission," *J. Lightwave Technol.,* vol. 8, no. 11, pp. 1716-1722, 1991.

[29] W. K. Marshall, J. Paslaski, and A. Yariv, "Reduction of relative intensity noise of the output field of semiconductor lasers due to propagation in dispersive optical fiber," *Appl. Phys. Lett.,* vol. 68, pp. 2496-2498, 1996.

[30] M. Nazarathy, J. Berger, A. J. Ley, I. M. Levi, and Y. Kagan, "Progress in externally modulated AM CATV transmission systems," *J. Lightwave Technol.,* vol. 11, no. 1, pp. 82-105, 1993.

[31] I. Jacobs, "Dependence of optical amplifier noise figure on relative-intensity-noise," *J. Lightwave Technol.,* vol. 13, No. 7, pp. 1461-1465, 1995.

[32] M. Movassaghi, M. K. Jackson, V. M. Smith, J. F. Young, and W. J. Hallam, "Noise figure of saturated erbium-doped fiber amplifiers: electrical versus optical measurement," in *Conference on Optical Fiber Communication OFC'97,* Vol. 6, 1997, OSA Technical Digest Series (Optical Society of America, Washington, D.C., 1997), paper WA2.

[33] M. Movassaghi, M. K. Jackson, V. M. Smith and W. J. Hallam, "Noise figure of erbium-doped fiber amplifiers in saturated operation," *IEEE Journal of Lightwave Technology,* vol. 16, no. 5, May 1998.

[34] M. Movassaghi, M. K. Jackson, V. M. Smith, J. F. Young, and W. J. Hallam, "Accurate frequency-resolved measurements of EDFA noise figure," in *Optical Amplifiers and Their Applications,* 1997 Technical Digest (Optical Society of America, Washington, D.C., 1997), paper TuD1.

[35] F. W. Willems, J. C. van der Plaats, and D. J. DiGiovanni, "EDFA noise figure degradation by amplified signal double Rayleigh scattering in erbium doped fibers," *IEE Electron. Lett.,* vol. 30, no. 8, pp 645-646, 1994.

[36] P. Bevington and D. Robinson, "*Data Reduction and Error Analysis for the Physical Sciences,*" McGraw-Hill, New York, 2nd ed, 1992.

[37] M. N. Zervas and R. I. Laming, "Rayleigh scattering effect on the gain efficiency and noise of erbium-doped fiber amplifiers," *IEEE J. Quantum Electron.*, vol. 31, no. 3, pp. 468-471, 1995.

[38] E. Desurvire, "An explicit analytical solution for the transcendental equation describing saturated erbium-doped fiber amplifiers," *Optical Fiber Technology*, no. 2, pp. 367-377, 1996.

[39] B. Pedersen, M. L. Dakss, B. A. Thompson, W. J. Miniscalco, T. Wei, and L. J. Andrews, "Experimental and theoretical analysis of efficient erbium-doped fiber power amplifiers," *IEEE Photon. Tech. Lett.*, vol. 3, no. 12, pp. 1085-1087, 1991.

[40] B. Pedersen, A. Bjarklev, O. Lumholt, and J. H. Povlsen, "Detailed design analysis of erbium-doped fiber amplifiers," *IEEE Photon. Tech. Lett.*, vol. 3, no. 6, pp. 548-550, 1991.

[41] M. Ohashi, and M. Tsubokawa, "Optimum parameter design of Er-doped fiber for optical amplifiers," *IEEE Photon. Tech. Lett.*, vol. 3, no. 2, pp. 121-123, 1991.

[42] M. Movassaghi and M. K. Jackson, "Design and modeling of saturated erbium-doped fiber amplifiers," to appear in *Tech. Dig. IEEE/LEOS Summer Topical Meet.*, San Diego, CA, USA, July 1999.

[43] M. Movassaghi and M. K. Jackson, "Simple and accurate modeling of high-efficiency saturated erbium-doped fiber amplifiers," submitted for publication to *J. Lightwave Technol* on July 27 1999.

[44] K. Bertilsson and P. Anderkson, "Modeling of Noise in Erbium-Doped Fiber Amplifiers in the Saturated Regime," *J. Lightwave Technol.*, vol. 12, No. 7, pp. 1198-1206, 1994.

[45] C. Giles, C. Burrus, D. DiGiovanni, N. Dutta, and G. Rayban, "Characterization of erbium-doped fibers and application to modeling 980-nm and 1480-nm pumped amplifiers," *IEEE Photon. Tech. Lett.*, vol. 3, no. 4, pp. 363-365, 1991.

[46] S. P. Craig-Ryan, B. J. Ainslie and C. A. Miliar, "Fabrication of long lengths of low excess loss erbium-doped optical fiber," *Electron. Lett.*, vol. 26, no. 3, pp. 185-186, 1990.

[47] S. Ovadia, "CNR limitations of Er-doped optical fiber amplifiers in AM-VSB video lightwave trunking systems," *IEEE Photon. Technol. Lett.*, vol. 9, no. 8, pp. 1152-1154, 1997.

[48] I. M. I. Habbab and L. J. Cimini, "Optimized performance of erbium-doped fiber amplifiers in subcarrier multiplexed lightwave AM-VSB CATV systems," *J. Lightwave Technol.*, vol. 9, no. 10, pp. 1321-1329, 1991.

[49] M. Movassaghi, M. K. Jackson and V. M. Smith, "DFB laser RIN degradation in CATV lightwave transmission," *Tech. Dig. IEEE/LEOS'98*, vol. 2, paper FB2, Dec 1998.

[50] M. Movassaghi, M. K. Jackson and V. M. Smith, "Dispersion-Induced RIN degradation and its impact on 1550nm AM video lightwave transmission systems, " revised manuscript under preparation for submission to *J. Lightwave Technol.*

[51] D. A. Atlas, R. Pidgeon, and F. Little, "Rayleigh backscatter effects on 1550-nm CATV distribution systems employing optical amplifiers," *J. Lightwave Technol.*, vol. 13, no. 5, pp. 933-946, 1995.

[52] A. Yariv, H. Blauvelt, D. Huff, and H. Zarem, "An experimental and theoretical study of the suppression of interferometric noise and distortion in AM optical links by phase dither," *J. Lightwave Technol.*, vol. 15, no. 3, pp. 437-443, 1997.

[53] R. D. Esman and L. Goldberg, "Simple measurement of laser diode spectral linewidth using modulation sidebands," *Electron. Lett.*, vol. 24, no. 22, pp. 1393-1395, 1988.

[54] A. Cartaxo, B. Wedding, and W. Idler, "Influence of fiber nonlinearity on the phase noise to intensity noise conversion in fiber transmission: theoretical and experimental analysis," *J. Lightwave Technol.*, vol. 16, no. 7, pp. 1187-1194, 1998.

Appendix A

Rate and Propagation Equations for 980nm-pumped EDFAs

In this appendix a more detailed analysis of the rate and propagation equations of a three level system is presented; this analysis leads to derivation of equations which correspond to equation (1.5)-(1.8) used for modeling 980nm-pumped EDFAs. All the analysis and derivations presented here closely follows Ref. [4].

A.1 Population Density of the Metastable level

As described in Section 1.4, for 980nm pumping, the EDFA behaves like a three level system. Figure A.1 shows these three levels as well as all the important transitions between them. In this figure R denotes the absorption rate (pumping rate) from level 1 to level 3, corresponding to the 980nm pumping. W_{12} and W_{21} are the absorption rate and the stimulated emission rate between levels 1 and 2, respectively. A_{21} represents the radiative spontaneous decay rate from level 2 to level 1, and A_{32} signifies the non radiative decay rate from level 3 to level 2. By definition level 1 is the ground level, level 2 is the metastable level characterized by a long lifetime τ, where $\tau = 1/A_{21}$, and level 3 is the pump level. The atomic rate equations corresponding to the populations of these three levels can be written as:

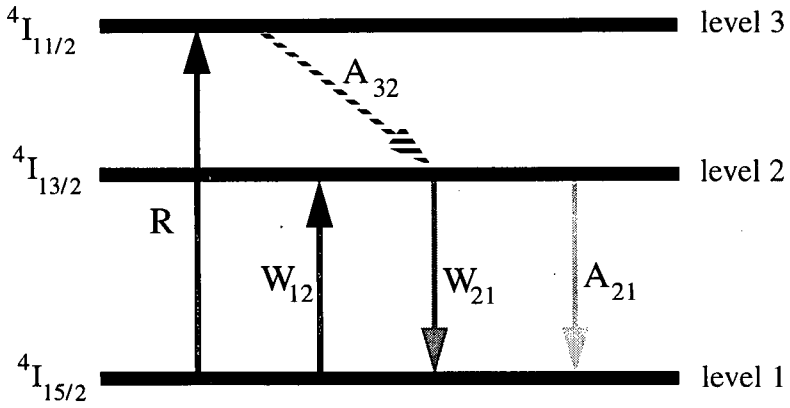

Fig. A.1. Energy level diagram corresponding to the first three energy levels of erbium in the glass host, and all the important transitions between these levels.

$$\frac{d\overline{N_1}}{dt} = -R\,\overline{N_1} - W_{12}\,\overline{N_1} + W_{21}\,\overline{N_2} + A_{21}\,\overline{N_2} \tag{A.1}$$

$$\frac{d\overline{N_2}}{dt} = W_{12}\,\overline{N_1} - W_{21}\,\overline{N_2} - A_{21}\,\overline{N_2} + A_{32}\,\overline{N_3} \tag{A.2}$$

$$\frac{d\overline{N_3}}{dt} = R\,\overline{N_1} - A_{32}\,\overline{N_3} \tag{A.3}$$

where $\overline{N_1}$, $\overline{N_2}$, and $\overline{N_3}$ are the densities of the electrons in the energy levels 1, 2, and 3, respectively. In the steady state regime of operation where the populations are time invariant, i.e., $\frac{d\overline{N_i}}{dt} = 0 \;\; (i = 1, 2, 3)$, and by considering the fact that $A_{32} \gg R$, the populations of the three levels can be written as:

$$\overline{N_1} = \rho\,\frac{1 + W_{21}\tau}{1 + (R + W_{12} + W_{21})\tau} \tag{A.4}$$

$$\overline{N_2} = \rho\,\frac{(R + W_{12})\tau}{1 + (R + W_{12} + W_{21})\tau} \tag{A.5}$$

$$\overline{N_3} = \frac{R}{A_{32}}\,n_1 \approx 0 \tag{A.6}$$

where $\rho = \overline{N_1} + \overline{N_2} + \overline{N_3}$ is the erbium ion density. Equation (A.6) shows that the pump level population, $\overline{N_3}$, is approximately zero. As described in Section 1.4, this is due to the fast non radiative decay rate of electrons from the pump level to the metastable level, and therefore

980nm-pumped erbium doped fibers can be analyzed by considering only levels 1 and 2.

For a single mode fiber, R, W_{12} and W_{21}, as a function of fiber coordinate z and radial axis r, are given as:

$$R = \frac{P_p(z)}{\tau\, P_p^{sat}}\,\psi_p(r) \tag{A.7}$$

$$W_{12} = \frac{\sigma_{sa}}{\tau\,(\sigma_{sa}+\sigma_{se})}\,\frac{P_s(z)}{P_s^{sat}}\,\psi_s(r) \tag{A.8}$$

$$W_{21} = \frac{\sigma_{se}}{\tau\,(\sigma_{sa}+\sigma_{se})}\,\frac{P_s(z)}{P_s^{sat}}\,\psi_s(r) \tag{A.9}$$

By substituting equation (A.7)-(A.9) into equation (A.5), the population density of the second level can be obtained as:

$$\overline{N_2}(r,z) = \rho(r)\,\frac{\dfrac{P_p(z)}{P_p^{sat}}\,\psi_p(r) + \dfrac{\sigma_{sa}}{\sigma_{sa}+\sigma_{se}}\,\dfrac{P_s(z)}{P_s^{sat}}\,\psi_s(r)}{1 + \dfrac{P_p(z)}{P_p^{sat}}\,\psi_p(r) + \dfrac{P_s(z)}{P_s^{sat}}\,\psi_s(r)} \tag{A.10}$$

Equation (A.10) corresponds to equation (1.8), with the difference that $n_2(r,z)$ is a normalized population and that it includes the ASE.

A.2 Propagation Equations for the Signal and Pump

When a light signal at wavelength λ with intensity I_s (power per area) passes through an active medium of length dz, and population densities of $\overline{N_1}$, for the ground level, and $\overline{N_2}$, for the metastable level, the intensity change dI_s is given by:

$$dI_s = (\sigma_e(\lambda)\overline{N_2} - \sigma_a(\lambda)\overline{N_1})\, I_s\, dz \tag{A.11}$$

where $\sigma_e(\lambda)$ is the emission cross section and $\sigma_a(\lambda)$ is the absorption cross section, both at the signal wavelength λ. For single mode propagation and for signal power of $P_s(\lambda)$, the light intensity distribution, $I_s(\lambda, r, \theta)$, in the fiber transverse plane is given as

$$I_s(\lambda, r, \theta) = P_s(\lambda) \frac{\psi_s(\lambda, r, \theta)}{\int_S \psi_s(\lambda, r, \theta) r dr d\theta}, \tag{A.12}$$

where θ is the azimuthal coordinate, and S denotes that the integral should be taken over the entire transverse plane. From equations (A.11) and (A.12), the propagation equation for the signal can be written as:

$$\frac{dP_s(\lambda)}{dz} = P_s(\lambda) \int_S \{\sigma_e(\lambda)\overline{N_2}(\lambda, r, \theta) - \sigma_a(\lambda)\overline{N_1}(\lambda, r, \theta)\}\bar{\psi}_s(\lambda, r, \theta) r dr d\theta \tag{A.13}$$

where $\bar{\psi}_s$ is the normalized mode power at wavelength λ defined as:

$$\bar{\psi}_s(\lambda, r, \theta) = \frac{\psi_s(\lambda, r, \theta)}{\int_S \psi_s(\lambda, r, \theta) r dr d\theta} = \frac{\psi_s(\lambda, r, \theta)}{\pi\, \omega_s^2(\lambda)} \tag{A.14}$$

By considering the radial symmetry of the optical mode, equation (A.13) simply leads to equation (1.5).

The above analysis also directly applies to the pump power. By considering that for 980nm pumping, $\sigma_e(\lambda)=0$, and that the excited state absorption for 980nm pumping occurs between levels 2 and 4, equation (1.6) is then easily obtained from equation (A.13) at $\lambda = 980\,\text{nm}$.

A.3 Propagation Equation for the ASE

The rate of creation of spontaneous emission power (P_{SE}) within an infinitesimal volume of active medium and within the frequency interval of $\Delta\nu$ is given by:

$$\frac{dP_{SE}}{dz} = 2\, P_0\, \sigma_e(\lambda) \int_S \overline{N_2}(r, \theta)\, \bar{\psi}_s(r, \theta)\, r\, dr\, d\theta \tag{A.15}$$

where $P_0 = h\nu\Delta\nu$ is the power of one spontaneous noise photon in bandwidth $\Delta\nu$. The total ASE power at any position z of the fiber is the sum of the ASE power from the previous sections of the fiber and the added spontaneous emission power at the position z. Therefore, from equation (A.15), which gives the rate of creation of the spontaneous emission and equation (A.13) which is the propagation equation for an optical beam propagating in the direction of positive z,

the propagation equation for the ASE propagating in positive z direction can be written as:

$$\frac{dP_{ASE}}{dz} = \int_S \{\sigma_e(\lambda)\overline{N_2}(\lambda, r, \theta)(P_{ASE}(\lambda) + 2P_0) - \sigma_a(\lambda)\,\overline{N_1}(\lambda, r, \theta)\}\overline{\psi}_s(\lambda, r, \theta)\,P_{ASE}\; rdrd\theta \tag{A.16}$$

By considering that ASE is also generated in the direction of negative z, equation (1.7) is easily obtained from equation (A.16).